Int J Earth Sci (Geol Rundsch) (2014) 103:1233–1262
DOI 10.1007/s00531-013-0948-7

ORIGINAL PAPER

Tertiary alkaline Roztoky Intrusive Complex, České středohoří Mts., Czech Republic: petrogenetic characteristics

Roman Skála · Jaromír Ulrych · Lukáš Ackerman · Emil Jelínek · Jaroslav Dostál · Ernst Hegner · Zdeněk Řanda

Received: 15 January 2013 / Accepted: 24 July 2013 / Published online: 12 September 2013

Abstract The České středohoří Mts. is the dominant volcanic center of the Ohře (Eger) rift zone. It hosts the Roztoky Intrusive Complex (RIC), which is made up of a caldera vent and intrusions of 33–28-Ma-old hypabyssal bodies of essexite–monzodiorite–sodalite syenite series accompanied by a radially oriented 30–25-Ma-old dike swarm comprising about 1,000 dikes. The hypabyssal rocks are mildly alkaline mostly foid-bearing types of mafic to intermediate compositions. The dike swarm consists of chemically mildly alkaline and rare strongly alkaline rocks (tinguaites). The geochemical signatures of the mildly alkaline hypabyssal and associated dike rocks of the RIC are consistent with HIMU mantle sources and contributions from lithospheric mantle. The compositional variations of essexite and monzodiorite can be best explained by fractional crystallization of parent magma without significant contributions of crustal material. On the other hand, the composition of monzosyenite, leuco-monzodiorite and sodalite syenite reflects fractional crystallization coupled with variable degrees of crustal assimilation. It is suggested that the parent magmas in the Ohře rift were produced by an adiabatic decompression melting of ambient upper mantle in response to lithospheric extension associated with the Alpine Orogeny.

Keywords Bohemian Massif · Cenozoic · Continental rift · Roztoky Intrusive Complex · Alkaline intrusions · Geochemistry

R. Skála (✉) · J. Ulrych · L. Ackerman
Institute of Geology, v. v. i., Academy of Sciences of the Czech Republic, Rozvojová 269, 165 00 Prague 6, Czech Republic
e-mail: skala@gli.cas.cz

E. Jelínek
Institute of Geochemistry, Mineralogy and Mineral Resources, Faculty of Science, Charles University in Prague, Albertov 6, 128 43 Prague 6, Czech Republic

J. Dostál
Department of Geology, Saint Mary's University, Halifax, NS B3H3 3C3, Canada

E. Hegner
Department für Geowissenschaften, Universität München, Theresienstraße 41, 80333 Munich, Germany

Z. Řanda
Nuclear Physics Institute, v. v. i., Academy of Sciences of the Czech Republic, 250 68 Řež, Czech Republic

Introduction

The European Cenozoic Rift System (ECRIS; Prodehl et al. 1995) is a major NE–SW-trending rift zone in western and central Europe. It extends from the Spanish Valencia Trough across the French Massif Central (Rhône Depression, Limagne Graben, Bresse-Saône Graben system), Black Forest and Vosges (Rhine Graben with Kaiserstuhl), Hegau, Urach and in the area of the Rhenish Massif (Lower Rhine Embayment, Hessen Depression), Vogelsberg, Rhön, Heldburger Gangschar) to the Bohemian Massif (Ohře/Eger Graben) (Wimmenauer 1974; Kopecký 1978; Wilson and Downes 1991; Ziegler 1994; Prodehl et al. 1995; Ulrych and Pivec 1997; Dèzes et al. 2004; Lustrino and Wilson 2007). The ECRIS lies mostly (volcanism in removed Lower Rhine Graben is missing) in the northern foreland of the Alps–Carpathian arc and is closely linked spatially and temporally to the Alpine Orogeny (e.g., Ziegler 1990, 1994; Prodehl et al. 1995).

Similar to other places in the ECRIS, magmatic rocks of the Ohře rift (OR) are typically anorogenic mildly silica-

undersaturated alkaline types (e.g., Ulrych et al. 2002, 2011; Lustrino and Wilson 2007). However, the OR contains, in addition to volcanic rocks, hypabyssal rocks of the high-level intrusions, which are rare in the other parts of the ECRIS. The presence of this kind of rocks can provide constraints on the genesis of the hypabyssal and subvolcanic level of volcanism and refine the ideas on the rift history. They can also contribute to a recent debate on whether intraplate magmatic activities in the ECRIS are related to mantle plumes or to passive adiabatic upwelling of sub-lithospheric mantle. A variety of processes have been suggested for the origin and development of the ECRIS magmatism (e.g., Lustrino and Carminati 2007 and references therein). They range from a model implying the presence of a "classic" mantle plume (Le Bas 1987; Wilson and Downes 1991), large-scale mantle plumes (Hoernle et al. 1995), channeled mantle plumes with the stem of the system located very far away beneath Cape Verde Island (Oyarzun et al. 1997) or Iceland (Wilson and Patterson 2001), a really limited deep mantle plumes (Goes et al. 1999), small plumes originated around the top of the mantle transition zone ("finger plumes"; Granet et al. 1995) or local passive diapiric upwelling (Lustrino and Wilson 2007), variably related to Alpine subduction processes (Foulger and Meyer 2007).

The purpose of this paper is to present whole-rock major and trace element concentrations, Sr–Nd isotope ratios and mineral chemical compositions of hypabyssal and associated dike rocks of the Roztoky Intrusive Complex (RIC), a major intrusive center of the České středohoří Mts. These data are used to constrain the petrogenesis, the mantle sources and tectonic geologic setting of the igneous activity.

Geological setting and characteristics of the Roztoky Intrusive Complex

Magmatism of the ECRIS in the Bohemian Massif (Czech Republic) represents the easternmost part of the Central European Volcanic Province (CEVP of Wilson and Downes 1991; Hoernle et al. 1995; Ulrych et al. 1999, 2011; Lustrino and Wilson 2007). In the Czech Republic, most voluminous Cenozoic magmatic activities occurred within the ENE–WSW-trending OR zone. The rift zone is thought to be a reactivated Variscan tectonic suture of the Bohemian Massif by the Alpine Orogeny. It is situated between the Moldanubian and Teplá-Barrandian blocks in the southeast and the Saxothuringian block in the northwest (Babuška and Plomerová 1992, 2001, 2010). Babuška et al. (2007) even invoke existence of the "triple junction" of the Saxothuringian—Teplá-Barrandian and Moldanubian lithospheric units in Western Bohemia.

In the Bohemian Massif, the magmatic rift system forms an arc-shaped belt extending over 500 km from the western to the easternmost parts of the massif (Franke 1989; Ziegler 1990, 1994; Fig. 1). The more pronounced western segment of the belt is a linear SW–NE-oriented structure bounded between the NW–SE striking Franconian and Labe-Odra wrench fault systems and contains the OR graben, which is about 180 km long and reaches a maximum width of 25–30 km. The OR contains a significant volume of volcanic rocks, which are locally associated with hypabyssal complexes. Further to the east and southeast, the volcanics occur in a more scattered form within the Labe-Odra wrench fault system (Fig. 1).

The crustal thickness in the Bohemian Massif is well constrained by numerous reflection and refraction seismic profiles (Hrubcová et al. 2008 and references therein) as well as receiver functions studies (Heuer et al. 2007; Geissler et al. 2008, 2012). These geophysical studies indicate the presence of a relatively shallow Moho (H_{RF} = 25–31 km) in the western part of the Bohemian Massif (e.g., Ziegler and Dézes 2006). This zone of thin crust, represented by the western OR graben, extends from the Western Bohemia/Vogtland region, where the Moho is shallowest (H_{RF} = 25–28 km), to the north and northeast toward Eastern Bohemia. The zone in Western Bohemia shows geochemical evidence (based on the fumarolic $^3He/^4He$ and CO_2 isotopic data) for ascending mantle-derived melts (Bräuer et al. 2005).

The distribution of Cenozoic volcanism associated with the OR is tectonically controlled. The two main volcanic centers within the OR are formed by the Doupovské hory Mts. and České středohoří Mts. complexes. They occur at the intersection of the OR with transverse NW–SE-trending faults (Fig. 1). The Doupovské hory Mts. Volcanic Complex, about 30 km in diameter, covering an area of nearly 600 km^2, crops out at the western part of the graben (Holub et al. 2010 and references therein). The České středohoří Mts. Volcanic Complex, further to the east, spreads over about 500 km^2 (Shrbený 1995).

The ages of igneous rocks emplaced in the OR range from late Cretaceous to Quaternary (~79 to 0.26 Ma; Ulrych et al. 2011). On the basis of K–Ar data and a paleostress chart, Ulrych and Pivec (1997) and Ulrych et al. (2011) defined three periods of Cenozoic magmatic activity in the OR: (1) pre-rift period (79–49 Ma), (2) syn-rift (42–16 Ma) and (3) late-rift period (16–0.26 Ma). This magmatic evolution in the OR is comparable to that of French Massif Central (Michon and Merle 2001). The volcanic rocks of the OR are mostly sodic SiO_2-undersaturated types forming two synchronous alkaline rock series: the dominant mildly alkaline basanite–trachyte series (MAS) and minor strongly alkaline nephelinite–phonolite series (SAS; Ulrych and Pivec 1997).

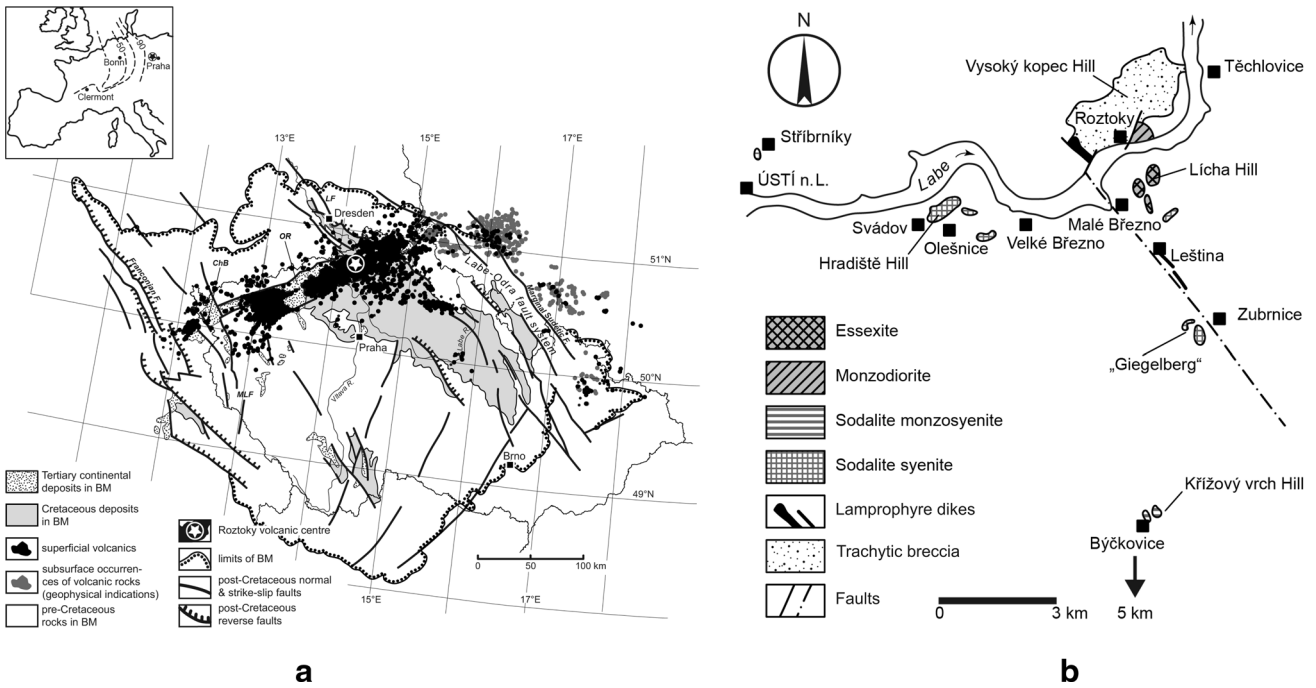

Fig. 1 Overview *map* of the Bohemian Massif with graben structures and Cenozoic igneous rocks of the Eger-Ohře graben. The Roztoky Intrusive Complex is indicated by *circled star*. *Inset* diagram shows lithospheric thickness contour lines in km (**a**). Detailed *map* showing the occurrence of different rock types of the Roztoky Intrusive Complex (**b**). *BM* Bohemian Massif, *ChB* Cheb Basin, *LF* Lusatian Fault, *MLF* Mariánské Lázně Fault, *OR* Ohře (Eger) Rift

The primitive mafic volcanic rocks from the OR have relatively uniform Sr–Nd–Pb isotope compositions with a common sub-lithospheric mantle source component (Blusztain and Hart 1989; Wilson et al. 1994; Lustrino and Wilson 2007; Ulrych et al. 2011). The isotopic and incompatible element characteristics of primitive mafic magmas of the OR are similar to those of the HIMU-type ocean island basalts (OIB) attributed to recycling of subducted oceanic crust in the upper mantle (Alibert et al. 1987; Lustrino and Wilson 2007) referred to the Common Magmatic Reservoir (CMR) by Lustrino and Wilson (2007).

The České středohoří Mts. represents an erosional relict within the OR graben. The largest center of magmatic activity of the České středohoří is the Roztoky Intrusive Complex (RIC; Fig. 1). The intrusive magmatic activity of the RIC lasted from ~33 to 25 Ma (Ulrych and Balogh 2000; Ulrych et al. 2011). The center is composed of an elliptical crater vent (3 × 1.5 km) filled with trachytic breccia and a cluster of trachytic to trachybasaltic and phonolitic dike intrusions. Large intrusion of olivine nephelinite occurs at northern margin of the RIC. Problematic carbonate dikes with Pb–Zn–Cu (Ag–Te) mineralization penetrating the monzodiorite intrusion at Roztoky (Pivec et al. 1998) show trace element and isotopic compositions similar to that known from late-carbonatites (Ulrych et al. 1997). Hypabyssal intrusions of monzodiorite, essexite, sodalite syenite as well as a radial dike swarm of lamprophyres and felsic differentiates occur in close proximity to the center (Ulrych 1983, 1998; Ulrych et al. 2006; Jelínek et al. 1989). The geophysical survey of Mrlina and Cajz (2006) found that essexite and monzodiorite intrusions at Roztoky form a single deep body that has a few protrusions reaching the surface.

The volcanic activities of the České středohoří Mts., stretching in the NE part of the Ohře Rift, are represented mostly by primitive alkali basaltic lavas, pyroclastics/volcaniclastics and rare intrusions of the similar composition. Four volcanostratigraphic formations of the latest Eocene to Late Miocene age (first two with an overlap of K–Ar ages) were recognized in this volcanic complex by Cajz et al. (1999), and Ulrych et al. (2002):

1. The Ústí Formation (age 36.1–25.5 Ma): Mg# 82–65, average 75; $^{87}Sr/^{86}Sr$ 0.70313–0.70353, $^{143}Nd/^{144}Nd$ 0.512738–0.512849, ε_{Nd} 2.8–4.8 comprising lavas and volcaniclastics of primitive basanitic, rarely olivine nephelinite composition. The basanitic magma is products of the initial phase of rifting, representing the near-primary magma of mantle source. A relatively rapid magma ascent (presence of angular mantle xenoliths), probably along the main rift-forming fault structures, can be supposed. Rejuvenation of tectonic movements associated with the development of the

Ohře Rift might have caused the periodically repeated activity of the magma chamber. The concept of pulsation character of magmatic chamber in a broader time span is broadly accepted (Bellon et al. 1998);

2. The Děčín Formation (age 30.8–24.7 Ma): Mg# 72–60, average 65, $^{87}Sr/^{86}Sr$ 0.70443–0.70465, $^{143}Nd/^{144}Nd$ 0.512979–0.512742 ε_{Nd} 1.5–2.6 comprising trachybasaltic lavas (prevailing trachybasalts transiting to basaltic trachyandesites) and pyroclastites, and hypabyssal bodies of the RIC (33.1–25.6 Ma; Ulrych and Balogh 2000). The Labe/Elbe valley is the only part of the České středohoří Mts. where the deeper levels of the volcanic pile, including hypabyssal bodies, are exposed. The trachybasaltic magma represents product influenced by crustal material. Geochemical and rheological characteristics result in the longer evolution within the independent high-level chamber and slower ascent of more acid magma accompanied by stopping and/or zone refinement. Both magma chambers occurring in different deep levels have been coeval, and feeding channels have been active at the same time. Similar time–coeval existence of two magma sources was presented by Wedepohl (1985) from Hessian Basins, Germany. The hypabyssal intrusions of the RIC represent probably the relatively older deep-seated product of this formation;
3. The Dobrná Formation (age 24.0–19.3 Ma): Mg# 79–70, average 75, $^{87}Sr/^{86}Sr$ 0.70365–0.70376, $^{143}Nd/^{144}Nd$ 0.512845–0.512847, ε_{Nd} 4.3–4.4 consisting of a primitive basanitic lava;
4. The Štrbice Formation (13.9–9.0 Ma): Mg# 80–69, average 75, $^{87}Sr/^{86}Sr$ 0.70365–0.70376, $^{143}Nd/^{144}Nd$ 0.512845–0.51247, ε_{Nd} 4.4–4.3 consisting of intrusions and lavas of basanitic composition.

One of the largest and well-exposed hypabyssal intrusions of the RIC, which is composed of monzodiorite, is rather heterogeneous (Fig. 2). It shows a steeply dipping magmatic rhythmic layering of rocks with variable grain size, texture and clinopyroxene/biotite ratios as well as bands of leuco-diorite and mela-monzodiorite. A similar vertical magmatic layering was described from the Monteregian Hills, Quebec, Canada, and it was interpreted to be the result of flowage differentiation, a process characteristic of the magma emplacement in a rift setting (Bhattacharji and Nehru 1972; Philpotts 1974; Eby 1984, 1985a, b). The RIC intrusions and related lamprophyric dikes contain enclaves of hornblendite cumulates, up to 50 cm in diameter.

The Doupovské hory Mts. Volcanic Complex is nearly coeval (~30 Ma) with the České středohoří Mts. Complex. The phaneritic rocks of this complex belong to the essexite–monzodiorite–monzosyenite association, with a composition similar to that of the RIC rocks. Here, clinopyroxenites and rocks of the melteigite–ijoilite–urtite series occur predominantly in the marginal parts of the complex (Holub et al. 2010).

The RIC is associated with a dike swarm consisting of about 1,000 dikes. They are mostly radially arranged, and the swarm has a radius of about 15 km. The dike system of the RIC is composed of: (1) lamprophyres (monchiquite,

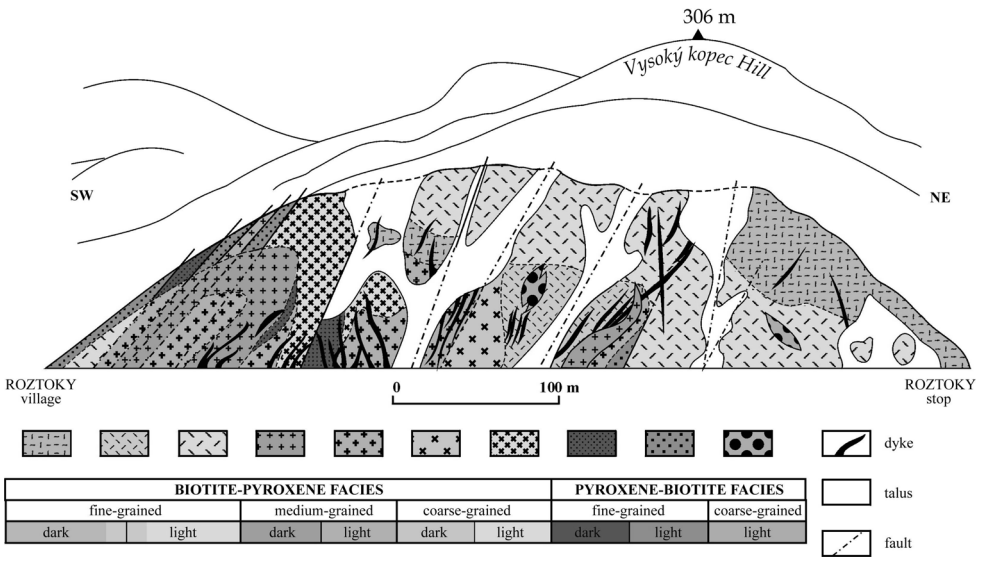

Fig. 2 Vertical section of the central part of the Roztoky monzodiorite body showing rhythmic, partly diffuse, layering. Exposure at the railroad cut near Povrly-Roztoky stop at the Ústí nad Labem–Děčín railroad line, Northern Bohemia. Biotite–clinopyroxene facies: (1) dark fine-grained, (2) dark medium-grained, (3) light fine-grained, (4) dark medium-grained, (5) light medium-grained, (6) dark coarse-grained, (7) light coarse-grained. Clinopyroxene–biotite facies: (8) fine- to coarse-grained (*dark in color*), (9) fine- to coarse-grained (*light in color*), (10) coarse-grained to pegmatitic (*light in color*), (11) dike rocks, (12) soils and hillside slopes, (13) faults indicated and supposed

camptonite; ~56 % of dikes), (2) medium derivatives (maenite of Rock 1991; local names "gauteite" and "bostonite"; ~28 %), (3) felsic derivatives (tinguaite; ~1 %), (4) basaltic rocks (~11 %) and (5) phonolites and trachytes (~4 %).

The hypabyssal rock series of the RIC exhibits many similarities in modal composition and geochemistry (e.g., the presence of essexites, sodalite syenites, both mafic and felsic dike rocks) with the Cenozoic volcanic complex of Kaiserstuhl in Germany (e.g., Wimmenauer 1974; Keller 1981).

Analytical methods

Twenty-four fresh samples were selected for this study. Whole-rock major element concentrations were determined by the wet chemical analysis methods at the Faculty of Science, Charles University in Prague, using wet chemical methods described in Johnson and Maxwell (1981) and Potts (1995). Analyses of the reference materials SY-4 CCRMP Canada and AGV-2 (USGS USA) yielded a total error of ±5 % (1σ).

The trace element analyses of whole-rock samples were carried out after modified total digestion in acids ($HF + HClO_4$) and borate fusion ($Na_2CO_3 + Na_2B_4O_7$) in platinum crucibles followed by solution nebulization using an ICP-MS PQ3 VG Elemental at Charles University in Prague. The analytical protocol and calibration strategy closely followed those described in Strnad et al. (2005). The relative standard deviation (RSD) of the ICP-MS data is 0.5–5 %. The accuracy as determined on the reference materials AGV-2 and BCR-2 (USGS, USA) measured as a ratio 100× sample/standard is 91–105 rel% for all elements.

Mineral analyses were carried out on a CAMECA SX 100 electron microprobe (EMP) at the Institute of Geology, v.v.i., Academy of Sciences of the Czech Republic, Prague. The analytical protocol used is the same of Ulrych et al. (2010).

The Sr–Nd isotope compositions were determined in the isotope laboratory at Universität München (Germany) according to the procedures outlined in Hegner et al. (1995). The $^{143}Nd/^{144}Nd$ ratios were determined with a Finnigan MAT 261 using a dynamic triple mass method and monitoring ^{147}Sm; Sm isotopes were determined in static data collection mode. The $^{143}Nd/^{144}Nd$ ratios were normalized to $^{146}Nd/^{144}Nd = 0.7219$ and $^{147}Sm/^{152}Sm = 0.56081$. The $^{143}Nd/^{144}Nd$ ratio of the in-house Ames Nd standard solution was 0.512142 ± 12 ($n = 35$), corresponding to 0.511854 in the La Jolla Nd reference standard material. The $\varepsilon_{Nd(t)}$ values were calculated with the parameters of Jacobsen and Wasserburg (1980). Present-day ratios for the chondrite uniform reservoir (CHUR) were the following: $^{147}Sm/^{144}Nd = 0.1967$, $^{143}Nd/^{144}Nd = 0.512638$ (Jacobsen and Wasserburg 1980; $^{143}Nd/^{144}Nd$ re-normalized to $^{146}Nd/^{144}Nd = 0.7219$). $^{87}Sr/^{86}Sr$ ratios were determined with a dynamic double mass method, monitoring ^{85}Rb, and normalized to $^{86}Sr/^{88}Sr = 0.1194$. The NIST 987 reference material yielded $^{87}Sr/^{86}Sr = 0.710230 \pm 11$ ($n = 22$).

Petrographic characteristics of hypabyssal and dike rocks of the Roztoky Intrusive Complex

The main petrographic characteristics of the hypabyssal rocks and dikes of the RIC are summarized in Table 8 of Appendix 1.

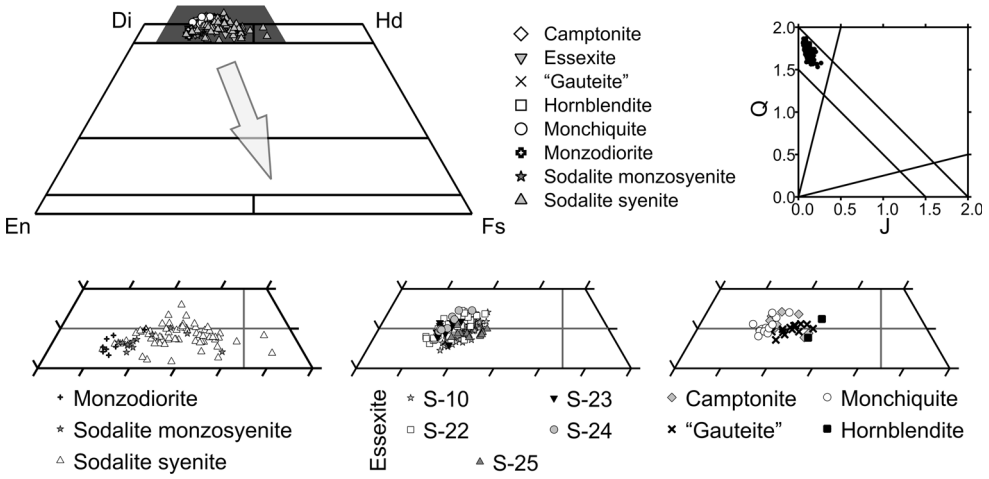

Fig. 3 Chemical composition and classification of pyroxenes of the hypabyssal and dike rocks of the Roztoky Intrusive Complex. The criteria of Morimoto et al. (1988) classify the pyroxenes based on Q–J diagram as Ca-pyroxenes. Except for two pyroxene grains, all compositions correspond to diopside. *Gray field* in the En–Fs–Di–Hd diagram at top left is zoomed into show the compositional variability of pyroxenes in detail in *three panels* at the *bottom*. Note the large spread in the composition of pyroxenes in sodalite (monzo)syenites, whereas those in essexites are relatively uniform

Hypabyssal rocks

Essexite (nepheline monzodiorite)

Three distinct petrographic types of the essexite were recognized as follows:

The *dark fine- to medium-grained type*, equigranular with hypidiomorphic texture is the most common (Fig. 16a of Appendix 2). It occurs in the central part of the intrusions. Fine grains of homogeneous plagioclase and natrolitized nepheline are the dominant felsic minerals. Next to them also larger laths of columnar zoned plagioclase and K-feldspar infilling of intergranular spaces occur rarely. Clinopyroxene is the predominant mafic mineral showing both sector and oscillation zoning. Biotite and amphibole (overgrowths or replacing of clinopyroxene) are also abundant.

The *light fine- to medium-grained type*, equigranular with prismatic granular texture, is common in marginal parts of the bodies, but also forms lenses in the central part (Fig. 16b of Appendix 2). The lath-shaped plagioclase is the dominant mineral. The relatively fresh columnar nepheline and K-feldspar fillings are relative less frequent. The most common mafic mineral is clinopyroxene, which is similar to that of the dark types. Biotite and amphibole are present in subordinate amounts.

The *porphyritic type* is characterized by the presence of 1–2-cm-long prismatic clinopyroxene phenocrysts enclosed in a medium-grained matrix composed of lath-shaped plagioclase and more rare alkali feldspar and nepheline.

Monzodiorite ("rongstockite")

The monzodiorite shows distinct compositional and textural variations including a magmatic rhythmic layering:

The *equigranular types* with hypidiomorphic prismatic textures are prominent in the intrusions. They are predominantly fine-grained passing into medium-grained varieties, which contain typical lath-shaped plagioclase (Fig. 16c, d of Appendix 2). Alkali feldspar is present in minor amounts as infilling between the plagioclase laths.

Table 1 Representative chemical analyses (in wt%) of clinopyroxene in hypabyssal and dike rocks of the Roztoky Intrusive Complex

Rock	SiO_2	TiO_2	Al_2O_3	Cr_2O_3	FeO^{tot}	MnO	MgO	CaO	Na_2O	K_2O	Total	En	Fs	Wo
Hypabyssal rocks														
Essexite	44.43	3.60	8.60	0.04	7.47	0.20	11.36	22.63	0.72	b.d.l.	99.05	36	13	51
	48.86	2.34	4.55	b.d.l.	6.80	0.18	12.73	23.14	0.96	b.d.l.	99.56	38	12	50
	45.25	3.47	7.37	0.06	7.08	0.27	11.83	23.24	0.74	b.d.l.	99.31	36	13	51
	50.33	0.97	2.42	b.d.l.	9.13	0.75	11.60	22.97	1.13	0.04	99.34	34	16	49
Monzodiorite	50.59	1.32	3.85	b.d.l.	6.81	0.05	14.08	22.49	0.49	b.d.l.	99.68	41	11	47
	49.61	1.89	4.27	b.d.l.	7.07	0.20	14.16	22.18	0.48	b.d.l.	99.86	41	12	47
Sodalite monzosyenite	44.37	3.87	7.34	0.04	9.44	0.19	10.52	22.22	0.68	0.06	98.72	33	17	50
	49.61	1.87	4.11	b.d.l.	7.82	0.23	12.84	22.38	0.52	0.06	99.42	38	13	48
	50.31	0.62	2.49	b.d.l.	12.86	0.93	9.27	21.05	1.38	b.d.l.	98.91	29	24	47
Sodalite syenite	49.87	1.38	4.65	b.d.l.	9.62	0.62	10.50	22.42	0.70	0.03	99.79	32	18	50
	45.92	3.29	8.00	b.d.l.	9.61	0.35	9.51	22.39	0.65	0.03	99.75	30	18	52
	48.58	2.02	4.33	0.02	7.49	0.23	13.72	23.25	0.47	b.d.l.	100.11	39	12	48
	52.25	0.57	1.78	b.d.l.	9.08	0.81	12.71	21.70	1.31	b.d.l.	100.20	38	16	46
	43.94	3.20	8.28	b.d.l.	10.64	0.25	10.10	22.27	1.04	b.d.l.	99.71	31	19	50
	45.74	2.21	6.80	0.05	11.79	0.39	9.73	22.17	1.13	0.16	100.17	30	21	49
Dike rocks and enclaves														
Camptonite	49.96	0.92	3.29	b.d.l.	9.96	0.58	11.69	23.41	1.01	b.d.l.	100.81	34	17	49
	46.52	2.93	6.84	b.d.l.	7.77	0.18	12.16	23.20	0.68	b.d.l.	100.28	37	13	50
Gauteite	44.56	3.58	8.20	b.d.l.	9.50	0.19	10.71	22.94	0.76	b.d.l.	100.42	33	17	51
	46.13	2.20	6.52	0.08	9.16	0.19	11.02	23.18	0.74	b.d.l.	99.22	33	16	51
Monchiquite	47.77	2.77	5.84	b.d.l.	6.77	0.24	12.72	22.97	0.61	b.d.l.	99.68	38	12	50
	44.90	3.79	7.78	b.d.l.	7.31	0.13	11.57	23.15	0.68	b.d.l.	99.31	36	13	51
Hornblendite	48.03	1.64	5.55	b.d.l.	10.07	0.27	11.04	22.39	1.20	b.d.l.	100.19	34	18	49
	45.80	2.26	9.41	b.d.l.	9.67	0.25	9.57	22.11	1.15	b.d.l.	100.22	31	18	51

Proportions of end-members are given in molar percentages

b.d.l. below detection limit

Short prismatic clinopyroxene and poikilitic biotite laths occur in subordinate amounts. Sector zoning of pyroxenes is rare. Hornblende occurs only rarely as overgrowths on clinopyroxene. The central part of the Roztoky monzodiorite body ("rongstockite" of Tröger 1935; Fig. 2) shows an unusual magmatic rhythmic layering. The banded rock contains numerous feldspathic (plagioclase 94 vol%, K-feldspar 4 vol%) medium-grained 2–5-mm-wide bands, which alternate with prevailing pyroxene–biotite dioritic to mela-monzodioritic bands (mafic/felsic bands ~3:2 vol%). A singular lens of clinopyroxene diorite to gabbro with relicts of olivine was also found in the central part of a rhythmic layered section. At the margins of the body, this type grades into a leucocratic, mostly fine-grained variety represented by sample S-1.

The *porphyritic types* with transitions to medium-grained types are characterized by large phenocrysts (up to 10 mm lengths) of clinopyroxene and biotite enclosed in a granular groundmass. Hornblende is very rare. Plagioclase forms equigranular grains displaying a concentric zoning and it prevails over K-feldspar occurring in intergranular spaces.

Sodalite (analcime) syenite

The syenitic rocks occur mainly in the outer parts of the RIC, as well as in some isolated intrusions up to 5–10 km from the center. They are predominantly fine-grained syenites or high-level intrusive trachytic rocks. Fine- to medium-grained rocks are usually equigranular, rarely with a hypidiomorphic granular texture (Fig. 16e of Appendix 2). Spaces between laths of feldspars are filled by isometric sodalite grains. Sodalite and/or analcime also occur as euhedral crystals. Micro-porphyritic rocks with phenocrysts of both plagioclases and sodalite are rare. Sodalite is nearly completely replaced by analcime. The most abundant mafic mineral is columnar clinopyroxene with common sector zoning. Hornblende occurs either as rare microphenocrysts or more commonly as phenocrysts (up to 10 mm) from disaggregated hornblendite enclaves (Fig. 16f of Appendix 2). The enclaves of *hornblendite* (up to 40 cm in size) are medium- to coarse-grained (Fig. 16g of Appendix 2). In addition to dominant kaersutite, the enclaves contain minor amounts of clinopyroxene (diopside), altered olivine and plagioclase with accessory amounts of titanite and apatite. Miarolitic cavities in the syenite are often filled by zeolites and carbonates.

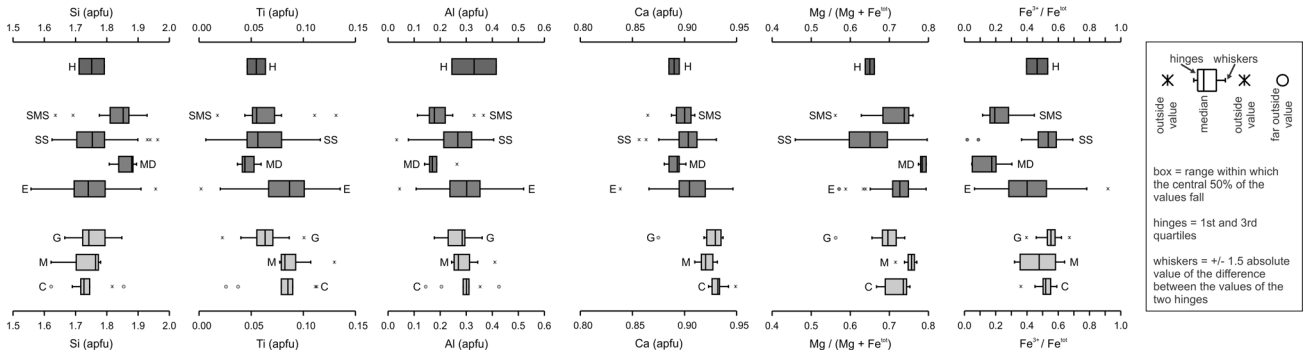

Fig. 4 *Box plots* showing the composition (in apfu) of pyroxenes in the hypabyssal and dike rocks of the Roztoky Intrusive Complex. Median values for Ca, Al and Ti contents increase from monzodiorite to sodalite monzosyenite, and sodalite syenite to essexite, whereas Si and Mg follows the opposite trend. *SMS* sodalite monzosyenite, *SS* sodalite syenite, *MD* monzodiorite, *E* essexite, *C* camptonite, *M* monchiquite, *G* "gauteite," *H* hornblendite

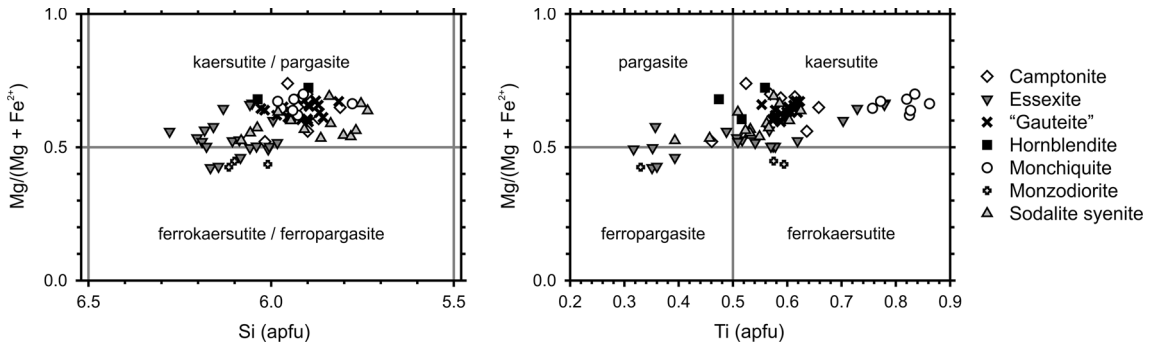

Fig. 5 Chemical composition and classification of amphiboles of the hypabyssal and dike rocks of the Roztoky Intrusive Complex adopting the scheme of Leake et al. (1997). The data correspond mostly to kaersutite though a few analyses represent ferrokaersutite, pargasite or ferropargasite

Sodalite-bearing monzosyenite to syenite

The sodalite-bearing monzodiorite forms one small intrusion at Býčkovice (Ulrych and Novák 1989). It is located about 15 km from the RIC (Fig. 1) and associated with a minor lamprophyre dike swarm. The rocks are mostly fine-grained, equigranular and have mineral characteristics similar to those of sodalite syenite (Fig. 16h of Appendix 2).

Dike rocks

Camptonite and monchiquite

Camptonite and monchiquite lamprophyre dikes (sensu Rock 1991 and Le Maitre 2002) are the most frequent dikes of the RIC area. Camptonite is composed of phenocrysts of kaersutite and phlogopite set in a fine-grained groundmass free of glass. Monchiquite is composed of phenocrysts of

Table 2 Representative chemical analyses (in wt%) of amphibole in hypabyssal and dike rocks of the Roztoky Intrusive Complex

Rock	SiO_2	TiO_2	Al_2O_3	Cr_2O_3	FeO	MnO	MgO	CaO	BaO	Na_2O	K_2O	F	Cl	Subtotal	O=F	O=Cl	Total
Hypabyssal rocks																	
Essexite	39.63	6.18	12.62	b.d.l.	12.71	0.24	10.70	11.92	b.d.l.	2.59	1.53	n.d.	n.d.	98.12	N/A	N/A	98.12
	40.34	4.95	10.97	b.d.l.	16.37	0.41	9.30	11.33	b.d.l.	2.73	1.84	n.d.	n.d.	98.24	N/A	N/A	98.24
	39.00	3.35	11.18	b.d.l.	18.21	0.46	8.72	11.88	0.05	2.42	1.92	1.33	0.06	98.58	0.56	0.01	98.01
Monzodiorite	35.60	6.60	13.60	b.d.l.	18.36	0.27	10.68	0.04	0.29	0.34	9.23	0.53	b.d.l.	95.54	0.22	0.00	95.32
	39.81	2.86	11.64	b.d.l.	20.03	0.38	7.96	11.51	b.d.l.	2.41	1.98	n.d.	n.d.	98.58	N/A	N/A	98.58
Sodalite syenite	39.14	5.12	13.21	0.07	10.46	0.18	13.15	12.15	b.d.l.	2.61	1.73	n.d.	n.d.	97.82	N/A	N/A	97.82
	40.00	4.66	11.56	b.d.l.	14.99	0.70	10.46	11.50	b.d.l.	2.80	1.72	n.d.	n.d.	98.39	N/A	N/A	98.39
	38.38	5.20	13.40	b.d.l.	11.45	0.19	12.67	12.19	b.d.l.	2.67	1.70	n.d.	n.d.	97.85	N/A	N/A	97.85
Dike rocks and enclaves																	
Camptonite	38.85	5.21	13.17	0.03	12.93	0.24	11.21	12.23	0.05	2.37	1.56	n.d.	n.d.	97.85	N/A	N/A	97.85
	39.37	5.43	12.50	b.d.l.	10.48	0.09	13.05	12.48	0.09	2.13	1.72	n.d.	n.d.	97.34	N/A	N/A	97.34
Gauteite	39.11	5.49	12.98	0.07	12.38	0.12	11.80	12.43	0.08	2.27	1.68	n.d.	n.d.	98.41	N/A	N/A	98.41
	39.12	4.88	12.94	b.d.l.	11.39	0.23	12.38	12.23	b.d.l.	2.27	1.84	n.d.	n.d.	97.28	N/A	N/A	97.28
Monchiquite	39.97	6.86	14.02	b.d.l.	9.88	0.00	11.37	12.75	b.d.l.	2.00	1.74	n.d.	n.d.	98.59	N/A	N/A	98.59
	39.24	7.26	12.59	b.d.l.	11.39	0.03	11.25	12.08	0.04	2.17	1.71	n.d.	n.d.	97.76	N/A	N/A	97.76
Hornblendite	39.80	4.59	12.55	b.d.l.	14.71	0.31	10.98	11.50	b.d.l.	2.25	1.50	n.d.	n.d.	98.19	N/A	N/A	98.19
	40.22	5.07	13.44	b.d.l.	9.71	0.14	13.78	12.00	b.d.l.	2.15	1.86	n.d.	n.d.	98.37	N/A	N/A	98.37

n.d. not determined, *N/A* not applicable, *b.d.l.* below detection limit

Table 3 Representative chemical analyses (in wt%) of mica in hypabyssal and dike rocks of the Roztoky Intrusive Complex

Rock	SiO_2	TiO_2	Al_2O_3	FeO^{tot}	MnO	MgO	CaO	BaO	Na_2O	K_2O	F	Cl	Subtotal	–F, Cl=O	Total
Hypabyssal rocks															
Essexite	34.98	10.36	13.30	16.16	0.21	10.71	0.03	2.90	0.78	7.83	1.18	0.04	98.48	0.51	97.97
	36.16	8.13	13.38	13.81	0.19	13.12	0.02	0.67	0.48	9.27	1.40	b.d.l.	96.63	0.57	96.06
	35.22	5.31	14.09	14.96	0.59	13.68	b.d.l.	1.29	0.59	9.25	2.38	0.04	97.40	1.01	96.39
	35.97	7.30	13.44	17.19	0.28	11.67	0.11	0.24	0.56	9.31	1.34	0.04	97.45	0.57	96.88
Monzodiorite	35.42	8.02	13.16	19.21	0.23	10.26	b.d.l.	0.72	0.38	9.09	0.47	0.03	96.98	0.20	96.77
	35.23	9.47	13.78	18.42	0.47	10.67	b.d.l.	1.08	0.44	8.72	0.50	b.d.l.	98.78	0.18	98.60
	34.80	4.83	14.55	21.82	0.39	9.63	b.d.l.	0.00	0.22	9.45	0.32	0.03	96.03	0.14	95.88
	35.33	6.43	14.27	20.06	0.28	10.39	b.d.l.	0.07	0.41	9.30	0.42	0.03	96.98	0.18	96.80
Sodalite syenite	34.80	7.44	13.68	15.41	0.32	13.05	b.d.l.	0.77	0.25	9.32	0.47	b.d.l.	95.51	0.20	95.31
	35.62	8.72	13.38	15.47	0.30	12.11	b.d.l.	1.32	0.53	8.76	0.37	0.03	96.60	0.16	96.44
Dike rocks:															
Camptonite	37.75	5.35	15.74	11.52	n.d.	15.46	n.d.	n.d.	n.d.	9.88	n.d.	n.d.	95.70	N/A	95.70
	38.02	6.8	16.1	8.24	n.d.	15.09	n.d.	n.d.	n.d.	10.43	n.d.	n.d.	94.68	N/A	94.68

Abbreviations as in Table 2

diopside and kaersutite in groundmass containing glass and/or analcime. It forms not only independent dikes but also "chilled margins" of camptonite dikes.

Maenite

Maenite covers local rock names "gauteite" and "bostonite" representing more acid medium derivatives (sensu Rock 1991), and maenites are often intimately associated with the camptonite–monchiquite dike suite (Rock 1991). Le Maitre (2002) supposes that maenite is a variety of trachyte and "bostonite" a leucocratic alkali feldspar syenite. Maenite contains phenocrysts of hastingsite, diopside, biotite, oligoclase, rarely also sodalite, in groundmass with rare glass. Transitional maenite types to camptonite as well as "bostonites" are from the RIC mentioned by Jelínek et al. (1989). "Bostonite" is composed mainly of oligoclase phenocrysts (rarely also diopside, hastingsite, biotite and sodalite) in fine-grained groundmass rich in both feldspars and sometimes also sodalite.

Tinguaite

Tinguaite and porphyric tinguaite dikes of phonolitic composition represent the most evolved rocks in the RIC. They were studied in detail by Ulrych et al. (2006).

Mineralogy and mineral chemistry

Clinopyroxene

Clinopyroxenes of all hypabyssal and dike rocks of the RIC occur as phenocrysts and/or grains in the matrix and correspond, following the classification of Morimoto et al. (1988), to aluminian ferroan *diopside* with about half of the grains being subsilicic and/or ferrian (Fig. 3). Selected analyses of clinopyroxenes are shown in Table 1. The ferroan pyroxenes (median Fe^{3+}/Fe_{tot} ~0.2) were found in monzodiorites and sodalite monzosyenites, the ferric types (median Fe^{3+}/Fe_{tot} ~0.5) occur in the most silica-deficient magmas like sodalite syenites and maenites, and in part also in camptonites; pyroxenes in essexites and monchiquites display an intermediate trend (median Fe^{3+}/Fe_{tot} ~0.4–0.45; see Fig. 4). Among hypabyssal rock types, some general compositional trends were observed: the contents of Ca, Al, and Ti increase from monzodiorite to sodalite monzosyenite, and sodalite syenite to essexite; Si and Mg follows the opposite trend. As a consequence, the contents of quadrilateral pyroxene end-members vary as well (Fig. 3). Many clinopyroxene phenocrysts show normal and/or sector zoning; in some cases, patchy zoning was observed as well. The sector zoning is mainly present in the dike rocks (Ulrych 1983). Concentric zoning usually

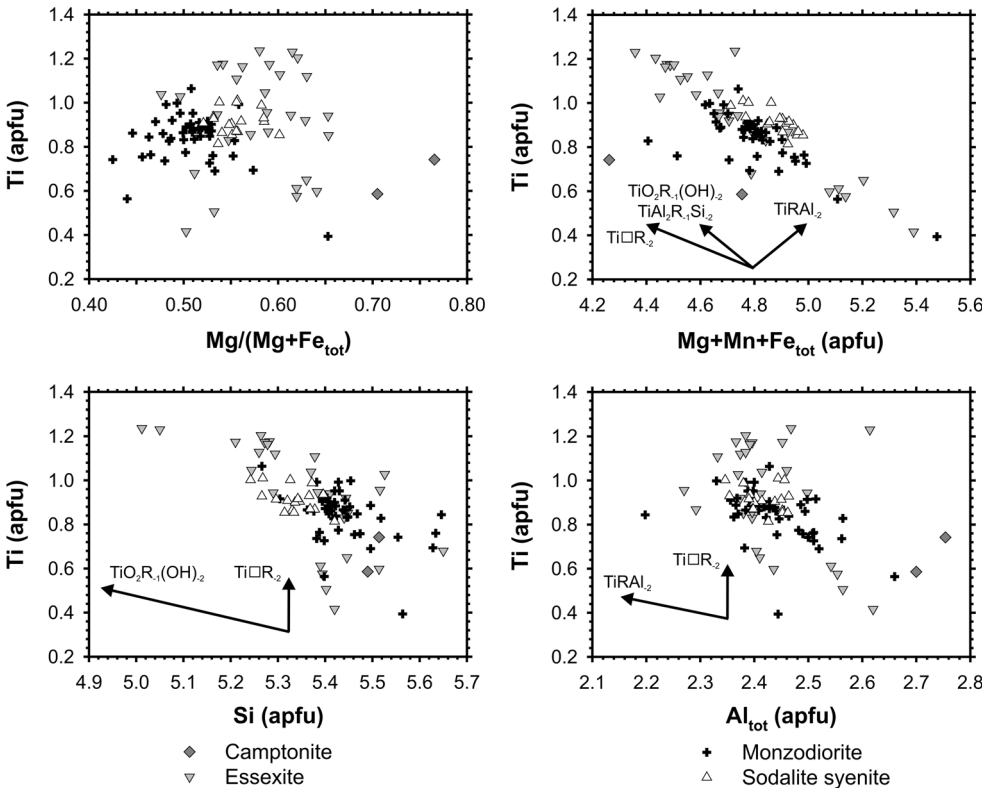

Fig. 6 Substitution vectors describing the composition of the micas found in the hypabyssal and dike rocks of the Roztoky Intrusive Complex

displays cores enriched in Mg and partly Si, whereas Al, Fe and Ti are depleted; Ca is constant across the entire grains.

Temperatures and pressures of pyroxene crystallization were calculated from their chemical composition and the chemical composition of the host rocks following Putirka (2008). Unfortunately, no reasonable estimate for composition of melt being at the equilibrium with crystallizing pyroxene has been available, so the numerical values can be used only for comparison purpose. The highest pressure and temperature have been calculated for pyroxenes in hornblendite enclaves. Slightly lower pT conditions can be assumed for hypabyssal rocks, and among them, the highest pressures and temperatures were calculated for essexite S-25. Pyroxenes in the dike rocks indicate even slightly lower temperatures and pressures of crystallization.

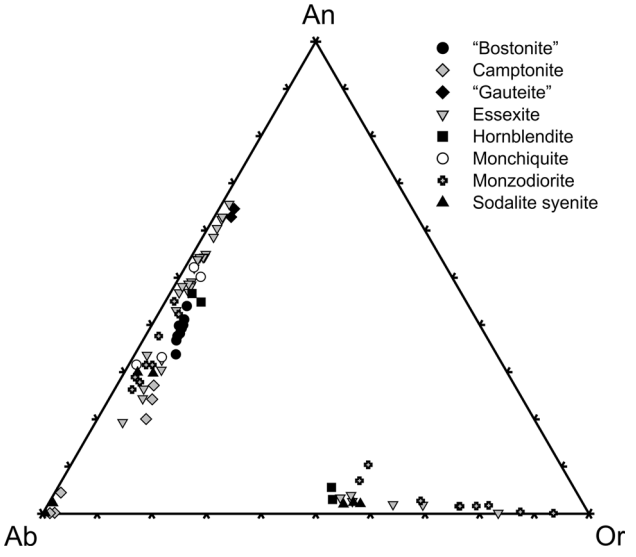

Fig. 7 Chemical composition of feldspars of the hypabyssal and dike rocks of the Roztoky Intrusive Complex

Amphibole

Amphiboles are abundant in lamprophyres and in sodalite syenite, where they occur as phenocrysts, groundmass and probably also xenocrysts from the disaggregated cumulates. They also occur in minor amounts in essexites and monzodiorites. According to the classification of Leake et al. (1997), amphiboles belong to the calcic series and predominantly correspond to potassian *kaersutite* or ferrokaersutite though a few analyses fall in the potassian titanian *pargasite* or ferropargasite (Fig. 5). Kaersutites in the matrix of monchiquites are typically enriched in TiO_2 (up to 7.5 wt%). Contents of F vary between 0.5 and 2.1 wt%, with Cl contents always below the EMP detection

Table 4 Representative chemical analyses (in wt%) of feldspar in hypabyssal and dike rocks of the Roztoky Intrusive Complex

Rock	SiO_2	TiO_2	Al_2O_3	Cr_2O_3	FeO^{tot}	MnO	MgO	CaO	BaO	Na_2O	K_2O	P_2O_5	Total	Ab	An	Or
Hypabyssal rocks																
Essexite	51.53	0.11	29.81	b.d.l.	0.20	b.d.l.	0.02	13.03	0.16	4.16	0.28	b.d.l.	99.30	36	62	2
	56.78	0.05	26.11	b.d.l.	0.38	b.d.l.	b.d.l.	9.31	0.11	6.45	0.53	b.d.l.	99.72	54	43	3
	61.08	0.07	23.42	b.d.l.	0.19	b.d.l.	b.d.l.	5.31	0.09	8.35	1.12	0.03	99.66	69	24	6
	64.52	0.12	19.27	0.03	0.23	0.04	b.d.l.	0.85	0.08	4.99	9.94	b.d.l.	100.07	42	4	55
Monzodiorite	56.07	0.08	27.10	0.03	0.33	b.d.l.	b.d.l.	9.23	0.47	6.51	0.69	0.03	100.54	54	42	4
	60.02	b.d.l.	23.98	0.04	0.28	b.d.l.	b.d.l.	5.93	0.25	8.03	0.69	b.d.l.	99.22	68	28	4
	64.59	b.d.l.	19.54	b.d.l.	0.17	b.d.l.	0.03	0.33	b.d.l.	2.22	13.40	0.03	100.31	20	2	79
Sodalite syenite	61.23	b.d.l.	23.73	0.05	0.24	b.d.l.	b.d.l.	6.35	b.d.l.	7.66	0.96	b.d.l.	100.22	65	30	5
	63.88	b.d.l.	18.98	b.d.l.	0.21	0.05	0.02	0.49	0.92	4.85	9.79	b.d.l.	99.19	42	2	56
	66.58	b.d.l.	20.62	0.07	0.21	b.d.l.	b.d.l.	0.48	0.02	11.39	0.14	0.05	99.56	97	2	1
Dike rocks and enclaves																
Bostonite	57.66	0.06	25.12	b.d.l.	0.41	b.d.l.	b.d.l.	8.42	0.08	6.44	0.89	0.04	99.12	55	40	5
Camptonite	61.91	b.d.l.	23.58	b.d.l.	0.06	b.d.l.	b.d.l.	5.65	b.d.l.	7.59	1.18	b.d.l.	99.97	66	27	7
	67.11	b.d.l.	20.15	0.04	0.23	0.05	0.04	0.00	b.d.l.	11.74	0.24	b.d.l.	99.60	99	0	1
Gauteite	52.02	0.12	28.55	0.11	0.54	b.d.l.	0.12	12.91	0.06	3.87	0.53	0.05	98.88	34	63	3
Monchiquite	54.24	0.10	28.06	b.d.l.	0.24	0.09	b.d.l.	11.30	0.17	5.53	0.29	0.05	100.07	46	52	2
	59.16	0.09	25.19	0.04	0.28	b.d.l.	b.d.l.	7.16	0.33	7.35	0.95	b.d.l.	100.55	62	33	5
Hornblendite	56.83	0.08	26.31	0.04	0.43	b.d.l.	b.d.l.	9.69	0.12	5.66	0.70	0.03	99.89	49	47	4
	63.96	0.08	19.21	b.d.l.	0.23	b.d.l.	0.02	0.63	1.45	5.25	9.06	b.d.l.	99.89	45	3	52

Proportions of end-members given in molar percentages. Abbreviation as in Table 2

limit. Representative analyses of amphiboles are summarized in Table 2.

The chemical composition of amphiboles allowed the estimation of pressures and temperatures of their formation. Temperatures were calculated applying semi-empirical thermometer of Otten (1984), and they vary between ~950 and 1,100 °C. The geobarometer of Schmidt (1992) yielded pressure values ranging from ~6 to ~8.5 kb.

Mica

Following IMA classification (Rieder et al. 1998), most micas correspond to ferroan phlogopite with few exception of magnesian–siderophyllite. In the diagram of Tischendorf et al. (2004, 2007), the majority of analyses fall into the field of *biotite*. A typical feature of all analyzed micas is elevated content of titanium; up to 10.5 wt% TiO_2 (~1.25 apfu in formulae based on 22 cations) was found in essexites (Table 3). Titanium enrichment is achieved mostly via $^{[6]}R^{2+} + 2(OH)^- \rightarrow {}^{[6]}Ti^{4+} + 2O^{2-}$ and $^{[6]}R^{2+} + 2^{[4]}Si^{4+} \rightarrow {}^{[6]}Ti^{4+} + 2^{[4]}Al^{3+}$ substitutions though other substitution vectors occur as well (Fig. 6). The temperatures of biotite crystallization, based on the thermometer of Henry et al. (2005), vary between 750 and 800 °C. Though the calculated values for temperature are semi-quantitative due to calibration of the geothermometer used, the overall trend is well-defined: the lowest temperatures were observed for monzodiorites, intermediate for sodalite syenites and the highest yet quite scattered for essexites.

Feldspar

In hypabyssal rocks, *plagioclase* is the major feldspar only in monzodiorite and essexite. It is distinctly zoned with $An_{26–66}$ in monzodiorite and essexite, and $An_{2–30}$ in sodalite syenite. Plagioclases in the dikes are compositionally variable with $An_{19–65}$ in mafic types of maenite ("gauteite") and $An_{33–44}$ in more felsic types ("bostonite"). *Alkali feldspar* occurs in monzodiorite and essexite both as phenocrysts and dispersed grains in matrix. Phenocrysts in monzodiorite range in composition between $Or_{55}Ab_{38}$ and $Or_{67}Ab_{29}$. Those in essexite are, compared to previous, enriched in potassium ($Or_{78}Ab_{19}$ to $Or_{65}Ab_{33}$). In a matrix, contrary to phenocrysts, feldspars correspond to solid solution varying from $Or_{83}Ab_{16}$ to $Or_{52}Ab_{44}$. In sodalite syenite, the chemical composition of alkali feldspar varies between Or_1Ab_{97} and $Or_{56}Ab_{41}$. Hornblendite contains both plagioclase ($An_{40–50}$) and alkali feldspar ($Or_{45}Ab_{50}$). Compositional variability of studied feldspars is shown in Fig. 7 and Table 4.

Using the calibrations of Putirka (2008), temperatures of crystallization were calculated from coexisting feldspar

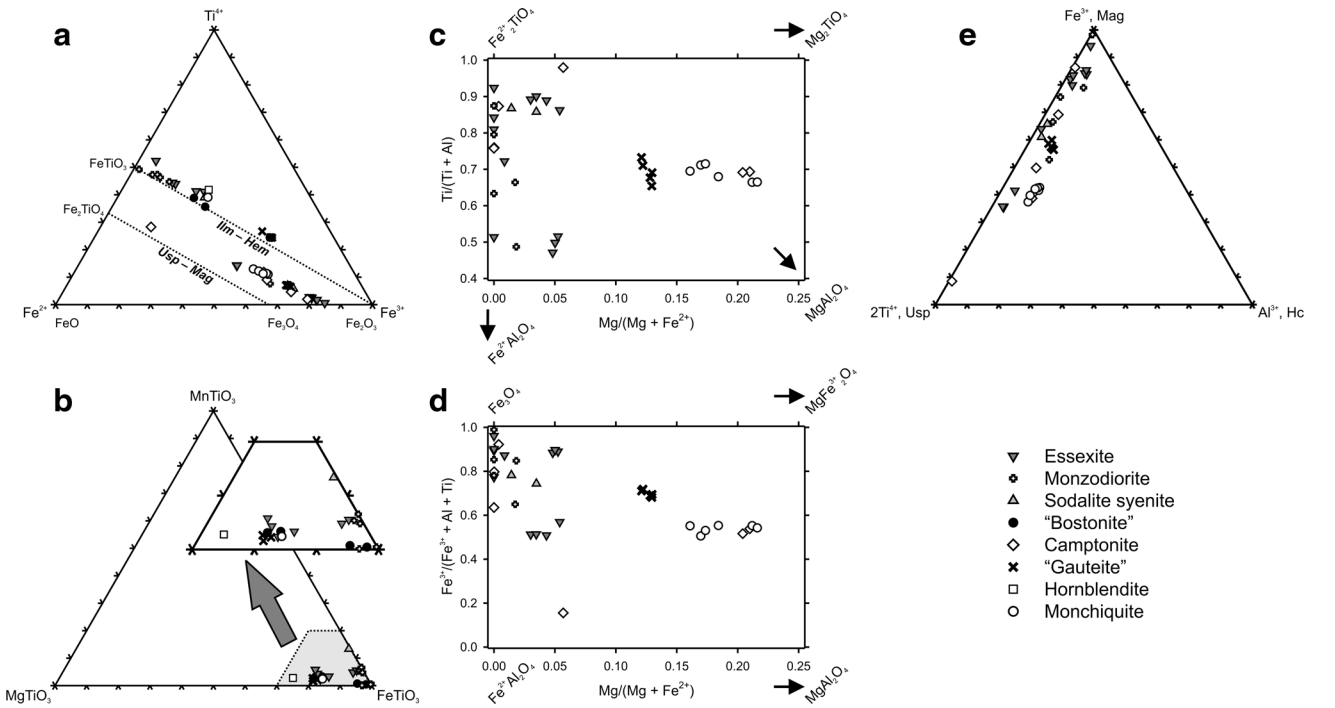

Fig. 8 Chemical composition of Fe–Ti oxide minerals of the hypabyssal and dike rocks of the Roztoky Intrusive Complex (**a**). Ternary diagram ilmenite–geikielite–pyrophanite (**b**) displays the compositional variation of ilmenites. A modification of Haggerty's spinel prism (**c**, **d**) is used to present the composition of spinel group minerals. Dike rocks display notably higher Mg content compared to hypabyssal ones. Ternary diagram magnetite–hercynite–ulvöspinel (**e**) illustrates a wide variation in the Usp content among titanium-rich magnetites

Table 5 Representative chemical analyses (in wt% and ppm, respectively) of apatite in hypabyssal and dike rocks of the Roztoky Intrusive Complex

	Hypabyssal rocks						Dike rocks and enclaves					
	Essexite		Monzodiorite		Sodalite syenite		Camptonite		Monchiquite		Hornblendite	
CaO	54.72	55.00	54.28	54.00	54.05	52.99	53.08	53.80	54.04	54.24	54.04	54.46
SrO	0.26	0.22	0.39	0.52	0.44	0.48	0.54	0.50	0.37	0.43	0.42	0.44
FeO	b.d.l.	0.16	0.14	0.16	0.16	0.16	0.32	0.30	0.24	0.30	0.24	0.29
MnO	b.d.l.	0.06	0.05	0.06	b.d.l.	0.08	0.04	0.06	0.07	0.08	0.08	0.07
MgO	b.d.l.	b.d.l.	0.06	0.21	0.09	0.24	0.24	0.24	0.13	0.07	b.d.l.	b.d.l.
Na_2O	0.04	0.13	b.d.l.	0.14	0.18	0.23	0.26	0.20	b.d.l.	0.00	0.04	b.d.l.
K_2O	b.d.l.	b.d.l.	b.d.l.	0.03	0.03	0.04	0.04	0.04	b.d.l.	0.03	b.d.l.	0.04
Al_2O_3	n.d.	n.d.	0.05	0.16	0.09	0.17	0.14	0.15	0.07	0.04	0.04	0.05
P_2O_5	41.86	41.94	40.97	40.47	41.50	41.70	40.74	40.46	39.81	39.96	40.12	40.56
SiO_2	0.31	0.51	0.10	0.20	0.17	0.22	0.22	0.21	b.d.l.	b.d.l.	0.11	0.16
SO_3	b.d.l.	0.45	0.21	0.47	0.63	0.38	0.76	0.92	0.09	0.10	0.63	0.97
CO_2	n.d.	n.d.	0.10	0.10	0.20	n.d.	0.19	0.19	0.15	0.15	0.15	0.15
F	4.01	4.60	0.81	1.26	3.19	2.42	1.78	1.10	2.37	0.74	2.10	1.66
Cl	0.17	b.d.l.	0.26	0.23	0.10	0.12	0.14	0.15	0.14	0.17	0.25	0.18
H_2O	n.d.	n.d.	1.78	1.93	0.48	1.95	2.44	2.07	2.75	2.68	1.88	1.76
Subtotal	101.37	103.07	99.20	99.94	101.31	101.18	100.93	100.39	100.23	98.99	100.10	100.79
–O=2F	1.69	1.94	0.34	0.53	1.34	1.02	0.75	0.46	1.00	0.31	0.89	0.70
–O=2Cl	0.04	N/A	0.06	0.05	0.02	0.03	0.03	0.03	0.03	0.04	0.06	0.04
Total	99.64	101.13	98.80	99.36	99.95	100.13	100.15	100.15	99.20	98.64	99.15	100.05
Zn			105		35	104	53		301		29.5	
Zr			1,616		1,278	2,124			1,164		912	
La			1,548		1,793	2,221	743		937		1,145	
Ce			3,033		2,956	3,731	1,563		1,938		1,863	
Pr			363				197		215		239	
Nd			1,699		1,171	1,473	934		1,067		860	
Sm			214		117	153	122		135		105	
Eu			51.8		33.4	44.4	34.2		37.5		28.4	
Gd			236		128	157	127		133		109	
Tb			19.4		10.9	15.0	11.4		12.0		8.59	
Ho			17.1		9.32	11.0	8.65		10.1		6.51	
Tm			5.68		4.30	4.39	3.07		3.25		2.82	
Yb			26.4		19.1	24.4	14.8		12.7		11.9	
Lu			3.40		2.82	3.45	1.89		1.83		1.72	
Hf			5.2		1.5	14.7	2.2		0.3		0.7	
Th			44.7		59.1	120	29.7		34.8		40.6	
U			7.96		7.89	14.9	4.98		6.02		8.62	
Σ(REE)			7,217		6,246	7,837	3,761		4,502		4,381	
$(La/Yb)_N$			42.1		67.33	65.3	36.0		52.9		69.0	
Th/U			5.61		7.49	8.09	5.95		5.77		4.71	
Zr/Hf			311		852	144	N/A		3,880		1,216	
Eu/Eu*			0.70		0.83	0.87	0.83		0.85		0.80	

Abbreviations as in Table 2

pairs: for essexites, the values range in a broad interval from ~900 to ~1,200 °C; for monzodiorites, temperatures vary between ~900 and ~1,000 °C; and for sodalite syenites, the procedure yields temperatures of ~1,000 and ~1,100 °C. Crystallization temperatures were further estimated from feldspar–liquid pairs; liquid was approximated as a respective host rock bulk chemical composition (Putirka 2008). Resulting temperatures are as follows:

Table 6 Major and trace element concentrations (in wt% and ppm, respectively) of rocks of the Roztoky Intrusive Complex

Sample	S-1	S-2	S-3	S-10	S-22	S-23	S-24	S-25	S-4	S-8	S-9	S-18	S-5
Locality	Roztoky, at gallery	Roztoky, below gallery	Roztoky, platform	Lícha Hill	Lícha Hill	Lícha Hill	Lícha Hill	Lícha Hill	Hradiště Hill	Stříbrníky	Olešnice valley	Hradiště Hill	Giegelberg
Rock	LMD	MD	MD	E	E	E	E	E	SS	SS	SS	SS	SS
SiO_2	51.08	43.57	46.62	45.72	43.86	53.46	47.96	41.32	48.88	49.30	53.02	49.42	51.04
TiO_2	1.75	2.73	2.64	3.08	3.53	1.71	2.94	4.01	1.68	1.72	0.97	1.73	1.72
Al_2O_3	17.42	18.36	17.94	15.47	15.07	18.53	17.07	13.40	18.53	18.04	19.94	18.64	17.29
Fe_2O_3	4.35	5.75	5.32	4.25	7.07	5.01	5.44	8.24	4.57	6.22	3.26	5.51	4.72
FeO	2.02	4.64	4.36	5.45	4.65	1.30	3.93	4.27	2.00	0.37	0.95	1.16	2.25
MnO	0.15	0.29	0.21	0.15	0.19	0.16	0.17	0.19	0.21	0.17	0.18	0.21	0.18
MgO	1.83	3.19	3.76	5.68	6.08	1.86	3.75	7.22	1.95	1.70	1.00	1.94	2.89
CaO	5.59	9.47	8.28	10.36	11.23	5.65	8.56	13.99	6.61	6.64	4.33	6.13	6.33
Na_2O	6.01	3.74	4.34	3.65	3.49	5.62	4.97	2.77	6.13	4.01	6.23	6.28	4.53
K_2O	4.00	2.42	2.37	3.92	2.63	4.72	3.62	2.35	4.00	3.87	5.49	3.67	3.49
P_2O_5	0.43	1.08	0.87	0.47	0.50	0.36	0.48	0.53	0.48	0.48	0.20	0.44	0.41
H_2O^+	2.21	1.46	1.09	1.25	1.33	1.17	0.71	1.17	3.11	3.26	3.25	3.51	3.44
H_2O^-	0.34	0.16	0.26	0.08	0.12	0.08	0.04	0.08	0.26	2.34	0.34	0.22	0.96
CO_2	2.58	2.78	1.75	0.11	0.09	0.14	0.08	0.20	1.35	1.63	0.63	0.84	0.67
Total	99.76	99.64	99.81	99.64	99.84	99.77	99.72	99.74	99.76	99.75	99.79	99.70	99.92
Rb	98.6	63.9	55.0	96.5	53.0	135	90.6	55.5	101	67.0	136	97.8	91.9
Cs	2.19	2.00	0.96	1.64	0.49	1.73	1.04	0.80	1.82	1.33	2.16	1.60	2.75
Sr	1020	1180	1490	820	844	908	960	791	1690	1530	1590	1550	1380
Ba	1100	732	976	813	800	1020	897	599	1290	1530	1380	1220	1260
Sc	5.84	9.49	8.38	26.4	27.3	5.77	15.4	37.3	3.82	4.23	1.24	4.47	7.83
Y	23.4	18.4	25.7	19.9	24.9	26.7	23.2	22.5	30.6	29.2	19.6	29.3	37.0
La	75.0	51.0	70.8	44.8	53.5	80.5	64.2	43.3	121	107	102	115	106
Ce	138	105	143	93.1	112	150	123	96.8	216	189	158	206	203
Pr	14.1	11.9	16.1	10.7	12.9	15.3	13.2	11.8	21.3	19.1	13.8	20.4	21.3
Nd	50.3	46.3	61.8	41.7	50.8	53.6	49.3	49.1	72.1	65.8	42.7	69.2	77.2
Sm	8.11	7.97	10.5	7.59	9.29	8.69	8.43	9.33	11.1	10.0	5.83	10.4	12.5
Eu	2.37	2.55	3.18	2.32	2.66	2.42	2.57	2.72	3.19	2.94	1.83	3.13	3.66
Gd	8.02	7.48	9.78	7.18	8.54	8.63	8.26	8.55	11.0	9.99	6.51	10.6	12.3
Tb	0.95	0.89	1.16	0.90	1.09	1.04	1.01	1.07	1.27	1.20	0.71	1.21	1.49
Dy	4.57	4.13	5.50	4.32	5.29	5.18	4.89	5.15	6.01	5.78	3.40	5.75	7.23
Ho	0.85	0.72	0.96	0.75	0.94	0.97	0.88	0.88	1.11	1.05	0.68	1.08	1.31
Er	2.51	1.96	2.69	2.11	2.61	2.95	2.51	2.39	3.32	3.09	2.13	3.22	3.87

Table 6 continued

Sample Locality Rock	S-1 Roztoky, at gallery LMD	S-2 Roztoky, below gallery MD	S-3 Roztoky, platform MD	S-10 Lícha Hill E	S-22 Lícha Hill E	S-23 Lícha Hill E	S-24 Lícha Hill E	S-25 Lícha Hill E	S-4 Hradiště Hill SS	S-8 Stříbrníky SS	S-9 Olešnice valley SS	S-18 Hradiště Hill SS	S-5 Giegelberg SS
Tm	0.33	0.24	0.32	0.26	0.34	0.39	0.31	0.28	0.43	0.40	0.30	0.40	0.50
Yb	2.08	1.40	2.00	1.58	2.09	2.58	2.01	1.73	2.73	2.63	2.09	2.66	3.28
Lu	0.31	0.19	0.30	0.23	0.30	0.39	0.30	0.25	0.41	0.40	0.32	0.39	0.480
Th	13.8	5.67	7.01	7.72	8.84	17.8	10.9	5.01	17.0	13.2	19.2	17.4	16.1
U	4.54	1.62	1.83	2.18	2.23	4.00	2.94	1.30	4.88	2.79	5.85	5.34	4.05
Zr	409	187	243	236	304	415	392	237	491	474	526	500	572
Hf	9.19	4.64	6.61	6.47	8.29	9.83	9.59	7.19	10.1	10.2	9.66	10.2	13.3
V	160	225	167	344	409	162	282	506	152	160	91	146	192
Nb	123	67	99	80	91	139	113	73	189	128	130	191	122
Ta	4.10	3.71	4.09	3.46	4.24	5.18	5.27	7.46	7.45	3.94	2.08	8.38	4.76
Cr	5.70	0.70	6.60	74.2	58.3	7.30	9.60	101	2.30	3.80	2.30	2.40	8.80
Co	9.20	26.6	16.2	31.3	34.1	9.20	21.4	41.1	10.2	9.80	4.70	9.40	13.0
Ni	8.60	17.6	10.6	37.9	27.4	3.40	8.30	35.7	22.2	5.20	9.00	2.00	10.3
Pb	4.44	34.4	29.9	2.86	20.8	0.38	23.2	3.06	6.91	0.830	51.0	8.79	29.5
Mg #	39	41	46	56	54	40	47	56	40	37	35	40	48.3
K/Rb	337	314	358	337	412	291	332	351	328	479	336	311	315
Rb/Sr	0.096	0.054	0.037	0.118	0.063	0.148	0.094	0.070	0.060	0.044	0.085	0.063	0.066
Th/U	3.04	3.50	3.83	3.54	3.96	4.45	3.72	3.85	3.49	4.73	3.28	3.26	3.96
Zr/Hf	44.5	40.3	36.8	36.5	36.7	42.2	40.9	33.0	48.9	46.5	54.5	49.2	42.9
Nb/Ta	30.0	18.1	24.2	23.1	21.5	26.8	21.4	9.8	25.4	32.5	62.5	22.8	25.6
ΣREE	307	242	328	218	263	333	281	233	471	419	341	449	454
La_N/Yb_N	25.9	26.1	25.4	20.3	18.4	22.4	22.9	18.0	31.9	29.2	35.0	31.0	23.2
Eu/Eu*	0.89	0.99	0.94	0.95	0.90	0.84	0.93	0.91	0.88	0.89	0.90	0.90	0.89

Table 6 continued

Sample	S-6	S-7	S-16	S-17	S-30	S-31	S-34	S-43	S-33	S-35	S-32
Locality	Giegelberg	Křížový vrch Hill	Křížový vrch Hill	Křížový vrch Hill	Dobkovice, quarry	Dobkovice, quarry	Těchlovice, quarry	Leština Brook	Těchlovice, quarry	Těchlovice, quarry	Těchlovice, quarry
Rock	H	SMS	SMS	SMS	M	C	C	C-G	G	G	Bo
SiO_2	36.68	49.96	49.42	49.34	45.88	47.84	46.36	42.68	53.68	52.72	53.86
TiO_2	4.58	1.78	1.90	1.92	3.22	2.13	2.93	2.97	1.78	1.70	1.30
Al_2O_3	8.59	18.18	18.22	17.69	14.99	16.15	16.25	13.83	17.53	17.61	17.16
Fe_2O_3	12.51	6.40	6.77	5.53	7.25	6.67	4.87	6.65	4.92	4.51	3.48
FeO	5.14	0.64	0.69	1.77	3.44	1.50	4.46	4.46	1.75	1.96	1.65
MnO	0.18	0.14	0.14	0.15	0.16	0.16	0.15	0.19	0.14	0.14	0.15
MgO	10.73	2.42	1.98	2.18	4.91	2.48	4.56	7.88	2.32	2.12	1.85
CaO	16.50	6.39	6.29	6.95	8.79	7.35	6.64	10.45	3.83	4.33	4.59
Na_2O	1.39	4.85	4.14	4.12	2.92	3.70	3.94	3.03	5.25	4.71	4.15
K_2O	0.78	4.47	4.21	3.77	4.09	4.07	4.80	2.15	4.89	6.29	4.24
P_2O_5	0.10	0.53	0.56	0.60	0.47	0.52	0.55	0.60	0.35	0.33	0.36
H_2O^+	1.07	1.74	2.35	2.24	2.99	2.28	3.27	2.59	2.96	2.38	0.41
H_2O^-	0.52	0.54	0.94	0.98	0.22	1.02	0.24	0.70	0.22	0.10	0.96
CO_2	1.08	1.69	1.12	2.45	0.23	3.56	0.66	1.28	0.11	0.67	5.45
Total	99.85	99.73	98.73	99.69	99.56	99.43	99.68	99.46	99.73	99.57	99.61
Rb	10.2	90.4	99.2	94.1	81.0	117	125	38.0	122	226	121
Cs	0.290	1.30	1.22	1.15	0.900	1.50	1.00	1.30	1.50	1.60	0.400
Sr	380	1310	1480	1480	641	1000	757	920	505	507	907
Ba	207	1270	1300	1220	781	937	1050	654	1420	1010	992
Sc	62.9	4.52	5.99	6.05	24.0	9.50	17.7	30.4	9.30	8.80	4.00
Y	16.4	24.6	24.8	25.3	20.8	25.4	21.2	23.9	22.5	22.3	25.1
La	16.8	81.0	80.8	82.6	48.7	76.9	57.0	61.6	72.0	69.4	79.1
Ce	43.5	148	149	151	101	147	114	128	131	127	148
Pr	6.20	15.2	15.4	15.8	11.8	16.4	12.8	14.6	13.8	13.6	15.7
Nd	29.5	54.5	54.7	56.7	45.8	59.3	48.2	56.9	48.9	47.7	56.0
Sm	6.52	8.81	8.92	9.28	8.58	9.84	8.44	10.3	8.06	7.89	9.32
Eu	1.97	2.59	2.63	2.68	2.48	2.89	2.51	3.02	2.25	2.19	2.52
Gd	5.88	8.72	8.83	8.99	8.21	9.88	8.15	9.74	8.01	7.77	9.16
Tb	0.79	1.04	1.06	1.07	1.03	1.23	1.03	1.22	0.99	0.95	1.08
Dy	3.83	5.04	5.05	5.23	4.84	5.62	4.88	5.51	4.66	4.48	5.25
Ho	0.65	0.91	0.91	0.94	0.85	1.00	0.87	0.96	0.86	0.84	0.97
Er	1.70	2.68	2.64	2.72	2.35	2.88	2.44	2.72	2.56	2.52	2.94
Tm	0.19	0.34	0.34	0.34	0.28	0.36	0.32	0.33	0.32	0.33	0.38

Table 6 continued

Sample	S-6	S-7	S-16	S-17	S-30	S-31	S-34	S-43	S-33	S-35	S-32
Locality	Giegelberg	Křížový vrch Hill	Křížový vrch Hill	Křížový vrch Hill	Dobkovice, quarry	Dobkovice, quarry	Těchlovice, quarry	Leština Brook	Těchlovice, quarry	Těchlovice, quarry	Těchlovice, quarry
Rock	H	SMS	SMS	SMS	M	C	C	C-G	G	G	Bo
Yb	1.18	2.16	2.20	2.22	1.81	2.37	1.93	2.05	2.26	2.13	2.53
Lu	0.170	0.320	0.320	0.320	0.270	0.340	0.280	0.290	0.330	0.310	0.380
Th	1.25	12.3	12.4	12.1	8.90	11.8	9.40	7.60	14.5	14.0	16.8
U	0.520	3.12	3.05	3.09	2.00	3.40	2.60	2.10	3.00	3.70	3.90
Zr	174	355	376	376	359	576	355	313	408	388	659
Hf	6.46	8.14	8.78	8.59	9.19	12.4	8.46	8.05	9.34	9.06	14.2
V	535	176	181	186	367	212	310	345	194	187	115
Nb	24.0	87.0	109	107	94.0	123	103	95.0	107	104	129
Ta	1.29	3.64	4.56	4.52	4.84	6.13	5.20	4.90	5.10	4.90	7.20
Cr	150	3.60	1.80	1.20	27.2	15.8	27.3	70.2	11.7	11.1	3.30
Co	64.3	10.0	8.80	10.0	30.6	16.5	27.3	37.4	13.8	12.9	6.90
Ni	103	5.30	3.20	1.60	22.3	14.8	39.0	75.0	10.0	10.0	5.00
Pb	5.04	13.7	29.5	9.62	6.20	7.00	6.50	16.8	10.2	13.6	14.5
Mg#	57.9	44.2	38.0	40.4	50.8	41.0	52.0	61.3	44.1	42.5	44.8
K/Rb	635	410	352	333	419	289	319	470	333	231	291
Rb/Sr	0.027	0.069	0.067	0.064	0.126	0.117	0.165	0.041	0.242	0.446	0.133
Th/U	2.40	3.95	4.08	3.92	4.45	3.47	3.62	3.62	4.83	3.78	4.31
Zr/Hf	26.9	43.6	42.8	43.8	39.1	46.6	42.0	38.9	43.7	42.8	46.4
Nb/Ta	18.6	23.9	23.9	23.7	19.4	20.1	19.8	19.4	21.0	21.2	17.9
ΣREE	119	332	333	340	238	336	263	298	296	287	334
La_N/Yb_N	10.2	26.9	26.3	26.7	19.3	23.3	21.2	21.6	22.9	23.4	22.4
Eu/Eu*	0.95	0.89	0.90	0.89	0.89	0.89	0.91	0.91	0.85	0.84	0.82

LMD leuco-monzodiorite, *MD* monzodiorite, *E* essexite, *SS* sodalite syenite, *H* hornblendite, *SMS* sodalite monzosyenite, *M* monchiquite, *C* camptonite, *C-G* camptonite to "gauteite," *G* "gauteite," *Bo* "bostonite." Mg# = 100 × Mg/(Mg + Fe^{2+}); for Fe^{3+}/Fe^{tot} = 0.15; La_N/Yb_N = chondrite-normalized ratio

essexite 1,050–1,180 and 1,270–1,340 °C (sample S-25); monzodiorite 1,060–1,100 and 1,250 °C; sodalite syenite 1,020 and 1,270–1300 °C; hornblendite 1,130–1,280 °C; camptonite 1,030 °C; maenite 1,080–1,100 °C; monchiquite 1,010–1,050 °C. Though the temperatures partially overlap, feldspars of dike rocks crystallized at generally lower temperatures.

Foid and zeolite

Nepheline is a common constituent of essexite and a minor phase in sodalite syenite. In tinguaites, it forms reddish orange phenocrysts and cloudy grains in matrix (with hauyne and sodalite; Ulrych et al. 2006). Nepheline of essexites, sodalite syenites as well as tinguaites corresponds to a Si-poor type of solid solution in the Ne–Ks–Qz–H_2O system at 700 °C and 1 kbar P_{H2O} (Wilkinson and Hensel 1994). *Sodalite* was probably the dominant primary mineral in the sodalite syenite but was almost completely replaced by *analcime*, which in addition also forms euhedral crystals in miarolitic cavities. In essexite, sodalite is rare. ***Natrolite*** is a common mineral of the matrix in sodalite syenite; it is formed by the decomposition of sodalite.

Carbonate

There are three groups of carbonates in the monzodiorite intrusion at Roztoky partly differing in chemical composition and in particular carbon and oxygen isotopic composition: (1) disputed primary ***calcite***, found only in carbonatized monzodioritic xenolith in trachytic breccia by Kopecký (1987a, b), (2) hydrothermal ***rhodochrosite dolomite*** and ***calcite*** related to epithermal tertiary Pb–Zn–Cu (Ag,Te) mineralization present in veins penetrating the monzodiorite (Pivec et al. 1998) interpreted by Kopecký (1987a, b) as products of residual solutions derived from a supposed carbonatite intrusion (late magmatic carbonatites C4 of Le Bas 1977), and (3) secondary chemically pure ***calcite*** in fissures associated with the alteration of the parental rock.

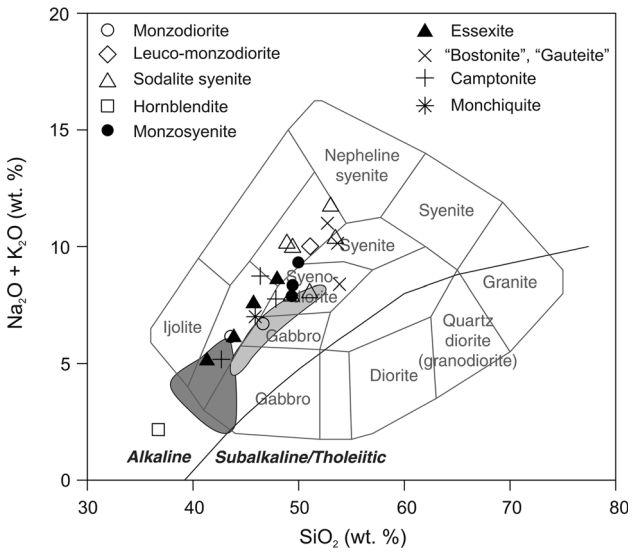

Fig. 9 Composition of hypabyssal and dike rocks of the Roztoky Intrusive Complex plotted to the classification diagram of Cox et al. (1979). *Dark gray* and *light gray* fields represent the composition of basanitic and trachybasaltic volcanic formations, respectively, from the České středohoří Mts. (Ulrych et al. 2002). These fields are shown to demonstrate the chemical affinity of studied RIC rocks to these formations

Kopecký (1987a, b) published isotopic data of the carbonate sample set. From this set, only one analysis of dolomitic carbonate (SrO ~1.0 wt%) of carbonatitized monzodiorite plots within the field of primary igneous carbonatites (PIC) as defined by Taylor et al. (1967). All other samples possess higher $\delta^{13}C$ and $\delta^{18}O$ values, plotting in the field of "carbonatite-associated carbonates," which generally do not represent primary igneous carbonate. The isotopic data of carbonates (Pivec et al. 1998) from the vein with epithermal mineralization in Roztoky show similar $\delta^{13}C$ but lower $\delta^{18}O$ values when compared with data reported by Kopecký (1987a, b). If a temperature of the Roztoky deposition between 200 and 280 °C (Pivec et al. 1998) for the hydrothermal vein carbonates is accepted, $\delta^{13}C_{fluid}$ values from ca. −3.0 to −5.0 ‰ and $\delta^{18}O_{fluid}$ values from ca. −3 to −7 ‰ (SMOW) can be calculated. The hydrothermal carbonates were formed during relative shallow hydrothermal circulation of low to medium salinity, and low $\delta^{18}O$ fluids supported by CO_2 influx of deep-seated origin. These carbonates are characterized by moderate REE contents (100–130 ppm), La/Yb ratios (49–63) and SrO (0.12–0.15 wt%) and Ba (0.22–0.88 wt%) contents and by $^{87}Sr/^{86}Sr$ ratios (rhodochrosite 0.7052; calcite and dolomite 0.7051; cf. parental monzodiorite (~0.7044) reflecting some crustal contamination). Data of $\delta^{13}C$ indicate probably minor admixture of sedimentary C in carbon of deep-seated origin, while the O isotope data point to participation of a $\delta^{18}O$ fluid of meteoric derivation (Ulrych et al. 1997).

Fe–Ti oxide

The ternary plot Ti–Fe^{2+}–Fe^{3+} (Fig. 8a) shows two major series, the ilmenite–hematite (rhombohedral s.s.) and magnetite–ulvöspinel (spinel s.s.; Buddington and Lindsley 1964). The position of the latter lies markedly off the ideal Usp-Mt line; this reflects the substantial isomorphic substitution of other spinel group end-members.

Three types of *ilmenite* were recognized (Fig. 8b): a pure ilmenite in monzodiorite and "bostonite," an ilmenite with low pyrophanite ($MnTiO_3$) content, hematite end-

members in essexite, monzodiorite and sodalite syenite, and a Mg-bearing ilmenite containing geikielite ($MgTiO_3$) and hematite end-members in essexite, maenite, monchiquite and hornblendite cumulates.

Magnetite occurs as (Fig. 8c–e): (1) pure magnetite associated with the decomposition of mafic minerals, (2) magnetite with medium contents of ulvöspinel end-member (Fe_2TiO_4) and low in magnesioferrite ($MgFe_2O_4$) and jacobsite ($MnFe_2O_4$) end-members in monzodiorite and essexite, (3) Ti-magnetite rich in the ulvöspinel end-member together with medium contents of magnesioferrite and jacobsite end-members in monzodiorite, essexite and sodalite syenite, (4) Ti-magnetite very rich in ulvöspinel and magnesioferrite end-members in monchiquite, camptonite and maenite. As illustrated in Fig. 8e, however, a few exceptions exist from this general trend. Ti-magnetite with a higher content of ulvöspinel and magnesioferrite end-members occurs in monchiquite.

Accessory minerals

Apatite compositionally corresponds to fluor-hydroxylapatite in monzodiorite, hornblendite and maenite, and to fluorapatite in sodalite syenite, essexite, camptonite and monchiquite. Its CO_2, SiO_2 and REE contents (Table 5) resemble the composition of apatites of carbonatite suites (Sommerauer and Katz-Lehnert 1985). *Titanite* forms at the expense of Ti-rich biotite in essexite. It commonly occurs also in hornblendite cumulates where it has high contents of REE (4,500–11,700 ppm).

Geochemistry of the hypabyssal and dike rocks of the Roztoky Intrusive Complex

Major and trace elements

Major and trace element concentrations of the main types rocks are listed in Table 6, and the data are plotted in the

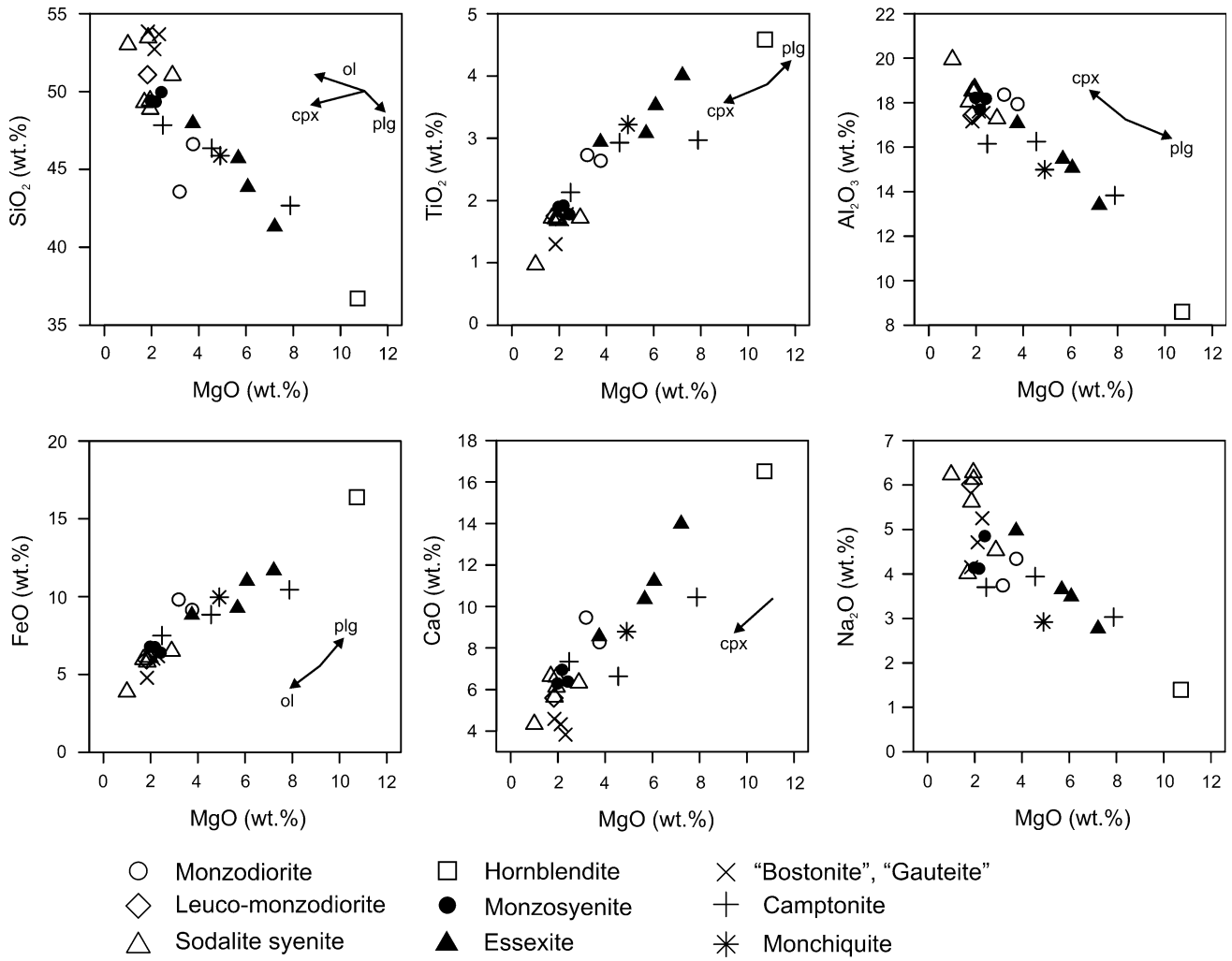

Fig. 10 Major element variation diagrams for hypabyssal and dike rocks of the Roztoky Intrusive Complex. Trends (*arrows*) of possible fractional phases from Guo et al. (2004)

diagram of Cox et al. (1979) in Fig. 9. The samples show a range in SiO_2 from 41 to 53 wt% and plot at high Na_2O and K_2O in the alkaline field; their Mg values fluctuate from 35.1 to 61.3 and alkali index A.I. ($Na_2O + K_2O/Al_2O_3$ mol%) 1.21–2.09:

(1) *hypabyssal mildly alkaline (tephritic)* series (essexite–monzodiorite–sodalite syenite) and hornblendite cumulate in sodalite syenite; (2) *mildly alkaline dike series* (MAS) (camptonite/monchiquite–maenite); and (3) *strongly alkaline dike series* (SAS) represented by tinguaite (Ulrych et al. 2006).

The major element variation with respect to MgO content is illustrated in Fig. 10. Positive correlation of TiO_2, FeO, CaO and negative correlations of SiO_2, Al_2O_3 and Na_2O with MgO suggest variable degrees of fractional crystallization as the main evolutionary process. Also, positive correlation exists between MgO and some compatible elements (e.g., Sc, Co; not shown).

The trace element variation in the hypabyssal intrusive rock series essexite–monzodiorite–sodalite syenite includes progressive enrichment in incompatible elements (e.g., rare earth elements—REE, large ion lithophile elements—LILE) and depletion of compatible elements (e.g., Cr, Co, Ni, Sc) and slight increase in light REE (LREE) relative to heavy REE (HREE).

Primitive mantle-normalized REE patterns (Fig. 11) of the hypabyssal rocks show a general enrichment in LREE with $(La/Yb)_N$ ratios varying from ~25 for monzodiorite to ~33 for sodalite syenite; hornblendite has the lowest LREE/HREE ratio of ~10. The REE patterns of lamprophyre dikes (Fig. 11) are similar to those of the hypabyssal rocks with the $(La/Yb)_N$ varying in the range of 18–22. Almost all the rocks exhibit a small negative Eu anomaly ($Eu/Eu^* = 0.9–1.0$). Primitive mantle-normalized incompatible element diagrams (Fig. 12) display a progressive enrichment from incompatible elements in monzodiorite to sodalite syenite. The slight depletion of P is typical of mafic rocks (essexite, monzodiorite), whereas a strong negative anomaly is typical of felsic types (e.g., sodalite syenite). When compared to the patterns of hypabyssal rocks, the hornblendite cumulate has substantially lower contents of LREE (Fig. 11) and other incompatible elements (Fig. 12), while it is enriched in Ti consistent with the accumulation of kaersutite/titanian magnetite.

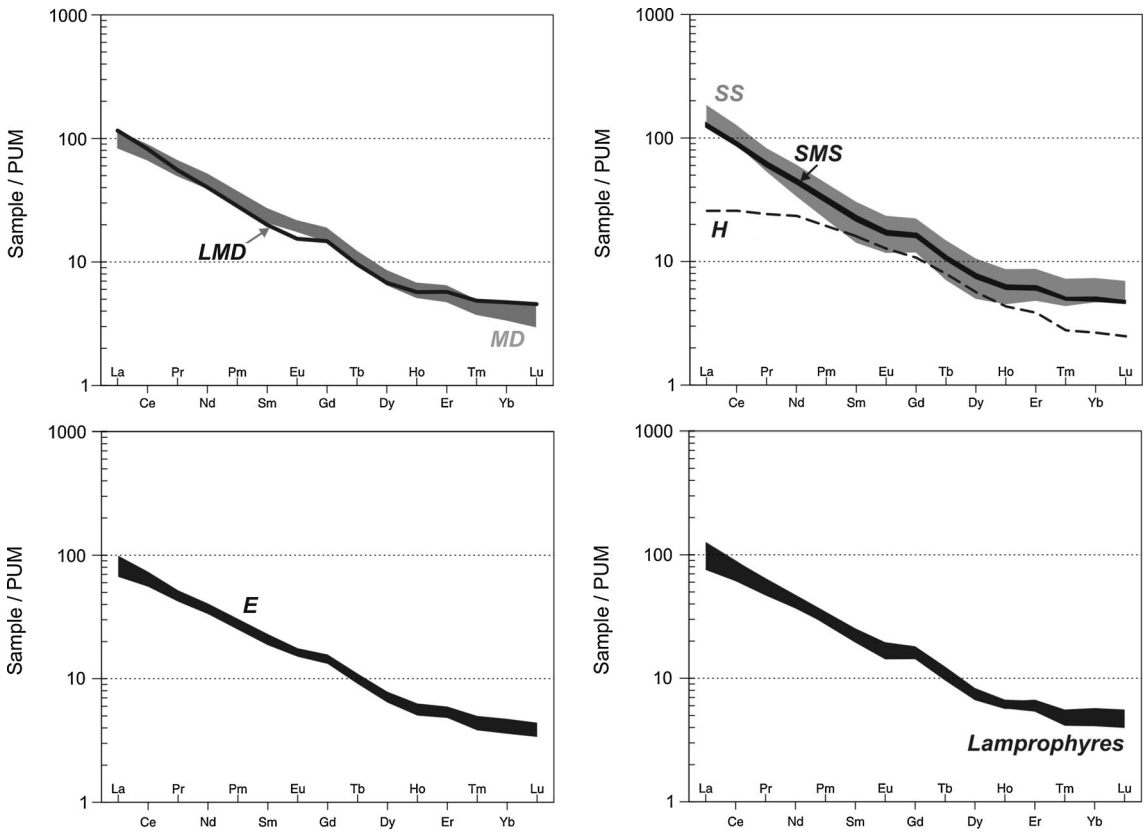

Fig. 11 Primitive mantle-normalized rare earth element (REE) patterns of hypabyssal and dike rocks of the Roztoky Intrusive Complex. Normalizing values from McDonough and Sun (1995). *E* essexite, *MD* monzodiorite, *LMD* leuco-monzodiorite, *SS* sodalite syenite, *SMS* monzosyeníte, *H* hornblendite

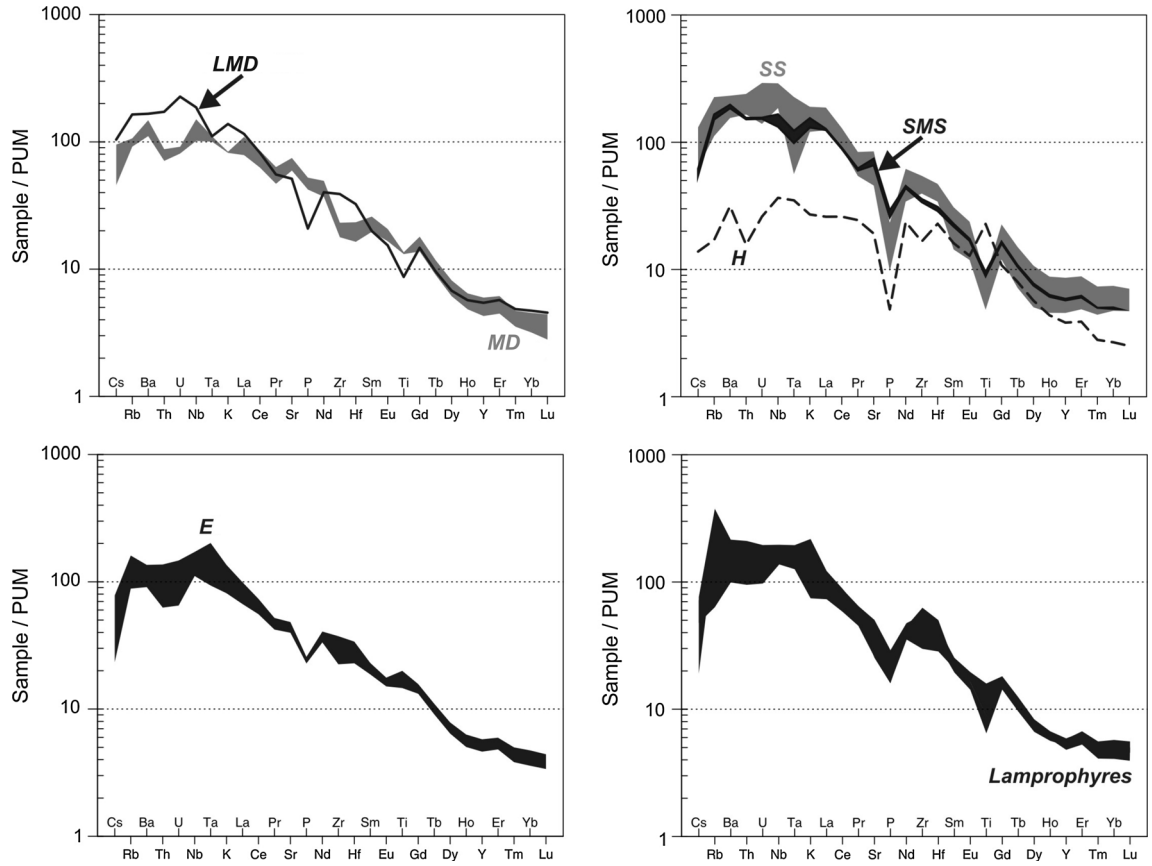

Fig. 12 Primitive mantle-normalized incompatible trace element patterns of hypabyssal and dike rocks of the Roztoky Intrusive Complex. Normalizing values from McDonough and Sun (1995). *ES* essexite, *MD* monzodiorite, *LMD* leuco-monzodiorite, *SS* sodalite syenite, *SMS* monzosyenite, *H* hornblendite

Among the hypabyssal rocks, the hornblendites have the highest K/Rb ratio (~635); other rocks display a broad variation between ~230 and ~480.

The lamprophyre dikes have similar concentrations of incompatible elements compared to the hypabyssal rock series, except Rb which is significantly enriched (Fig. 12). The trace element patterns show depletions in Cs, Rb, P, Ti and enrichment in Zr and Ba relative to elements with similar compatibility. Enrichment in incompatible elements and depletion in compatible elements are even more pronounced in felsic rock types. Their patterns also show depletion in P and Ti and enrichment in Nb and Zr.

Most of the hypabyssal rocks and associated dikes are distinctly differentiated as indicated by their low MgO contents and Mg#. However, those with MgO contents over 7 wt% and/or Mg# >56 show PM-normalized trace element patterns consistent with primitive volcanic rocks of the OR and resemble those of HIMU-OIB with enrichment in high-field-strength elements (HFSE) and frequently a negative K anomaly.

The Zr/Hf ratios of the RIC rocks vary in a range from of 33 to 55 with the exception of the hornblendite cumulate (~26). The lower ratios in felsic types might be due to the late-magmatic (or post-magmatic) fluids producing Zr minerals. Various Zr-bearing minerals were identified at other localities in the region by Ulrych et al. (1992).

$^{87}Sr/^{86}Sr$ and $^{143}Nd/^{144}Nd$ isotopes

Initial $^{87}Sr/^{86}Sr$ ratios have been recalculated to 30 Ma (Table 7). Hypabyssal rocks range from 0.70375 (sodalite syenite) to 0.70503 (sodalite monzosyenite). The $^{143}Nd/^{144}Nd$ ratios show a large variation and initial ε_{Nd} values ranging from +0.7 to +3.4. Except for the sodalite monzosyenite samples, the samples plot at the lower end of the field for 42–16-Ma syn-rift volcanic rocks of Ulrych et al. (2011) and are in some cases less radiogenic in their Nd isotopic composition (Fig. 13). However, there are distinct differences among similar rock types. For example, sodalite syenites show a large variation in ε_{Nd} from +1.3 to +3.3. In contrast, sodalite monzosyenites exhibit very homogeneous Sr–Nd isotopic compositions, but strong decoupling between $^{87}Sr/^{86}Sr$ and $^{143}Nd/^{144}Nd$ ratios in that their Sr isotopic composition departs from the mantle array (Fig. 13). Lamprophyric dikes have Sr–Nd isotopic compositions overlapping those of hypabyssal rocks.

Table 7 Rb–Sr and Sm–Nd isotope data for hypabyssal and dike rocks of the Roztoky Intrusive Complex

Sample	Rock type	Rb (ppm)	Sr (ppm)	$^{87}Rb/^{86}Sr$	$^{87}Sr/^{86}Sr$	$^{87}Sr/^{86}Sr(30)$	Nd (ppm)	Sm (ppm)	$^{147}Sm/^{144}Nd$	$^{143}Nd/^{144}Nd$	$^{143}Nd/^{144}Nd(30)$	εNd(30)
S-1	Monzodiorite	99	1,022	0.28	0.704456 ± 10	0.70434	50.3	8.11	0.0975	0.512723 ± 10	0.51270	2.0
S-2	Monzodiorite	64	1,183	0.16	0.704396 ± 9	0.70433	46.3	7.97	0.104	0.512750 ± 9	0.51273	2.5
S-3	Leucomonzodiorite	55	1,486	0.11	0.704576 ± 11	0.70453	61.8	10.51	0.103	0.512732 ± 11	0.51271	2.2
S-4	Sodalite syenite	101	1,686	0.173	0.703852 ± 10	0.70378	72.1	11.07	0.0928	0.512775 ± 11	0.51276	3.1
S-5	Sodalite syenite	92	1,385	0.19	0.704473 ± 8	0.70439	77.2	12.52	0.0980	0.512683 ± 11	0.51266	1.3
S-6	Horneblendite	10	380	0.078	0.704015 ± 10	0.70398	29.5	6.52	0.134	0.512756 ± 10	0.51273	2.5
S-7	Sodalite monzosyenite	90	1,311	0.20	0.705120 ± 10	0.70503	54.5	8.81	0.0977	0.512712 ± 11	0.51269	1.8
S-8	Sodalite syenite	70	1,534	0.13	0.704198 ± 10	0.70414	65.8	10.01	0.0919	0.512736 ± 10	0.51272	2.3
S-9	Sodalite syenite	136	1,591	0.247	0.704311 ± 11	0.70421	42.7	5.83	0.0825	0.512783 ± 11	0.51277	3.3
S-10	Essexite	97	820	0.34	0.704314 ± 10	0.70417	41.7	7.59	0.110	0.512732 ± 9	0.51271	2.2
S-16	Sodalite monzosyenite	99	1,475	0.19	0.705090 ± 8	0.70501	54.7	8.92	0.0985	0.512709 ± 11	0.51269	1.8
S-17	Sodalite monzosyenite	94	1,478	0.18	0.705113 ± 11	0.70503	56.7	9.28	0.0990	0.512706 ± 11	0.51269	1.7
S-18	Sodalite syenite	98	1,549	0.18	0.703830 ± 11	0.70375	69.2	10.43	0.0911	0.512794 ± 11	0.51278	3.4
S-22	Essexite	53	844	0.18	0.704191 ± 11	0.70411	50.8	9.29	0.111	0.512744 ± 10	0.51272	2.4
S-23	Essexite	135	908	0.430	0.704883 ± 8	0.70470	53.6	8.69	0.0980	0.512655 ± 11	0.51264	0.7
S-24	Essexite	91	960	0.27	0.704284 ± 10	0.70417	49.3	8.43	0.103	0.512721 ± 11	0.51270	2.0
S-25	Essexite	56	791	0.20	0.703904 ± 9	0.70382	49.1	9.33	0.115	0.512780 ± 11	0.51276	3.1
S-30	Monchiquite	81	641	0.37	0.704164 ± 9	0.70401	45.8	8.58	0.113	0.512743 ± 10	0.51272	2.4
S-31	Camptonite	117	1,002	0.338	0.704220 ± 10	0.70408	59.3	9.84	0.100	0.512740 ± 10	0.51272	2.4
S-32	Bostonite	121	907	0.386	0.704659 ± 10	0.70449	56.0	9.32	0.101	0.512661 ± 10	0.51264	0.8
S-33	Gauteite	122	505	0.699	0.704282 ± 9	0.70398	48.9	8.00	0.0989	0.512687 ± 10	0.51267	1.3
S-34	Camptonite to gauteite	125	757	0.478	0.704266 ± 9	0.70406	48.2	8.44	0.106	0.512735 ± 9	0.51271	2.2
S-35	Gauteite	226	507	1.29	0.704764 ± 9	0.70421	47.7	7.89	0.100	0.512665 ± 10	0.51265	0.9
S-43	Camptonite	38	920	0.12	0.704437 ± 10	0.70439	56.9	10.30	0.109	0.512751 ± 10	0.51273	2.5

^{143} Nd/^{144}Nd ratios are normalized to $^{146}Nd/^{144}Nd = 0.7219$. Measured $^{143}Nd/^{144}Nd$ ratio of the in-house Ames Nd standard solution was 0.512142 ± 12 ($N = 35$), corresponding to 0.511854 in the La Jolla Nd reference material. The $\varepsilon_{Nd(30)}$ values were calculated with the parameters of Jacobsen and Wasserburg (1980). Present-day values for the chondrite uniform reservoir (CHUR): $^{147}Sm/^{144}Nd = 0.1967$, $^{143}Nd/^{144}Nd = 0.512638$ (Jacobsen and Wasserburg 1980; $^{143}Nd/^{144}Nd$ re-normalized to $^{146}Nd/^{144}Nd = 0.7219$). $^{87}Sr/^{86}Sr$ ratios are normalized to $^{86}Sr/^{88}Sr = 0.1194$. The NIST 987 reference material yielded $^{87}Sr/^{86}Sr = 0.710229 \pm 8$ ($N = 22$)

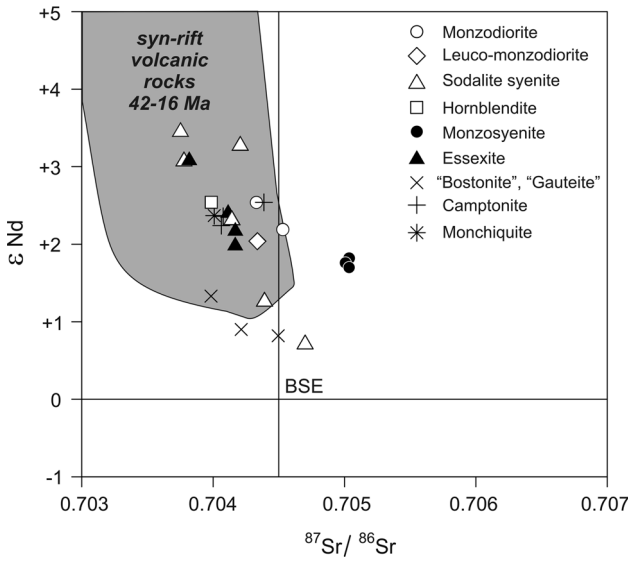

Fig. 13 Initial $^{87}Sr/^{86}Sr$ and $^{143}Nd/^{144}Nd$ isotope ratios for ca. 30-Ma-old hypabyssal and dike rocks of the Roztoky Intrusive Complex. The *gray field* of 42–16-Ma syn-rift volcanic rocks uses data of Cenozoic volcanic rocks from Ulrych et al. (2011), Lustrino and Wilson (2007) and Ulrych (unpublished data). *BSE* Bulk Silicate Earth. *Symbols* as in Fig. 10

Discussion

The RIC suite belongs to the volcanic series of the České středohoří Mts., which represents an integral part of the ECRIS. The RIC hypabyssal rock series (essexite, monzonite, sodalite syenite, questionable carbonatites) accompanied by dike rock suite (camptonite–tinguaite) and other intrusions as olivine nephelinite, tephrite/basanite, phonolite have the only analogue within the ECRIS: similar rock series of Kaiserstuhl in the Rhine Graben, Germany (Wimmenauer 1974; Ulianov et al. 2007). Compositionally, the extrusive volcanic rocks of the České středohoří Mts. resemble those of the Massif Central in France (Wilson et al. 1995) and the German Volcanic Province (Lustrino and Wilson 2007). Other partly analogous rift-related rock associations in Europe are known from Oslo Graben in Norway (Dons and Larsen 1978) and Serra de Monchique, Portugal (Rock 1978). The RIC rock suite shows close textural as well as chemical similarities to that of the Monteregian Province rift (St. Lawrence rift system), Quebec, Canada. The origin of all these alkaline rock suites is usually explained by fractional crystallization of a mantle-derived magma (Eby 1984, 1985a, b, 1987).

The hypabyssal rock suites of the RIC formed by mildly alkaline essexite–monzodiorite–sodalite syenite series and dikes, which appear to be closely genetically related. This is indicated by: (1) Radial orientation of a dike swarm around the core composed of hypabyssal intrusions of monzodiorite, essexite and partly also sodalite syenite (Hibsch 1926; Shrbený 1969; Ulrych et al. 1983; Kopecký 1978); (2) The comparable ages of hypabyssal rock series (33–28 Ma) and dike rocks (30–25 Ma; Ulrych and Balogh 2000); (3) Covariations of major and trace element contents of the hypabyssal intrusions and dikes (Ulrych et al. 1983; Ulrych 1998; Jelínek et al. 1989); and (4) Overlap of the Sr–Nd isotope composition of the hypabyssal rocks and dikes.

Tinguaites representing the singular member of the strongly alkaline series were studied in detail by Ulrych et al. (2006). The rocks are rich in alkali and other incompatible elements and have high contents of Cl and SO_3 concentrated in sodalite and nosean. The large variation of $^{87}Sr/^{86}Sr_{30}$ from 0.70335 to 0.70419 and εNd_{30Ma} values of +2.1 to +4.3, indicating a moderately depleted mantle source, are comparable to that of other dike rocks of the RIC. The chemically evolved composition of tinguaites was attained via melt differentiation at shallow crustal levels with limited assimilation of crust. Their K–Ar ages of 31–28.5 Ma and chemical geochemical characteristics support their synchronous origin with the rocks of the RIC.

The intrusions of RIC are texturally and compositionally heterogeneous. The significant heterogeneity of individual intrusions is also demonstrated by alternation in bands of various grain sizes, texture (porphyritic vs. equigranular), contents of mafic minerals (leucocratic vs. mesocratic) and clinopyroxene/biotite ratio. These variations are probably due to flowage differentiation during the emplacement of the intrusion at a deeper crustal level. The steeply dipping magmatic layering is indicative of rocks crystallizing in extensional rift conditions. Bhattacharji (1966), Bhattacharji and Nehru (1972), Philpotts (1974) and Eby (1984, 1985a, b) suggest that such inhomogeneity (vertically dipping rhythmic layering) and flowage differentiation of hypabyssal rocks are characteristic form of their emplacement under the riftogenic conditions, e.g., in the Monteregian Hills, Canada).

The variations in major elements, petrography and mineral chemistry indicate that the RIC suite, including hypabyssal rocks of intrusions and both dike series, may be derived from parent magmas of alkali basalt affinities by fractional crystallization. For RIC suite, whole-rock TiO_2, CaO, FeO, Ni and Co contents show good positive correlation with MgO, while SiO_2, Al_2O_3, Na_2O, Ba and Sr are negatively correlated with the same oxide (Figs. 10, 14). All these trends could be explained by the fractionation of clinopyroxene, plagioclase, olivine and apatite (e.g., Guo et al. 2004). The presence of kaersutite + diopside ± olivine, fluorapatite, labradorite, titanite cumulates (e.g., sample S-6) in sodalite syenites, and some lamprophyres partly support this model. However, fractionation of amphibole (kaersutite) from the parental melt would lead to decrease in Ba, Sr or MREE (medium rare earth elements)

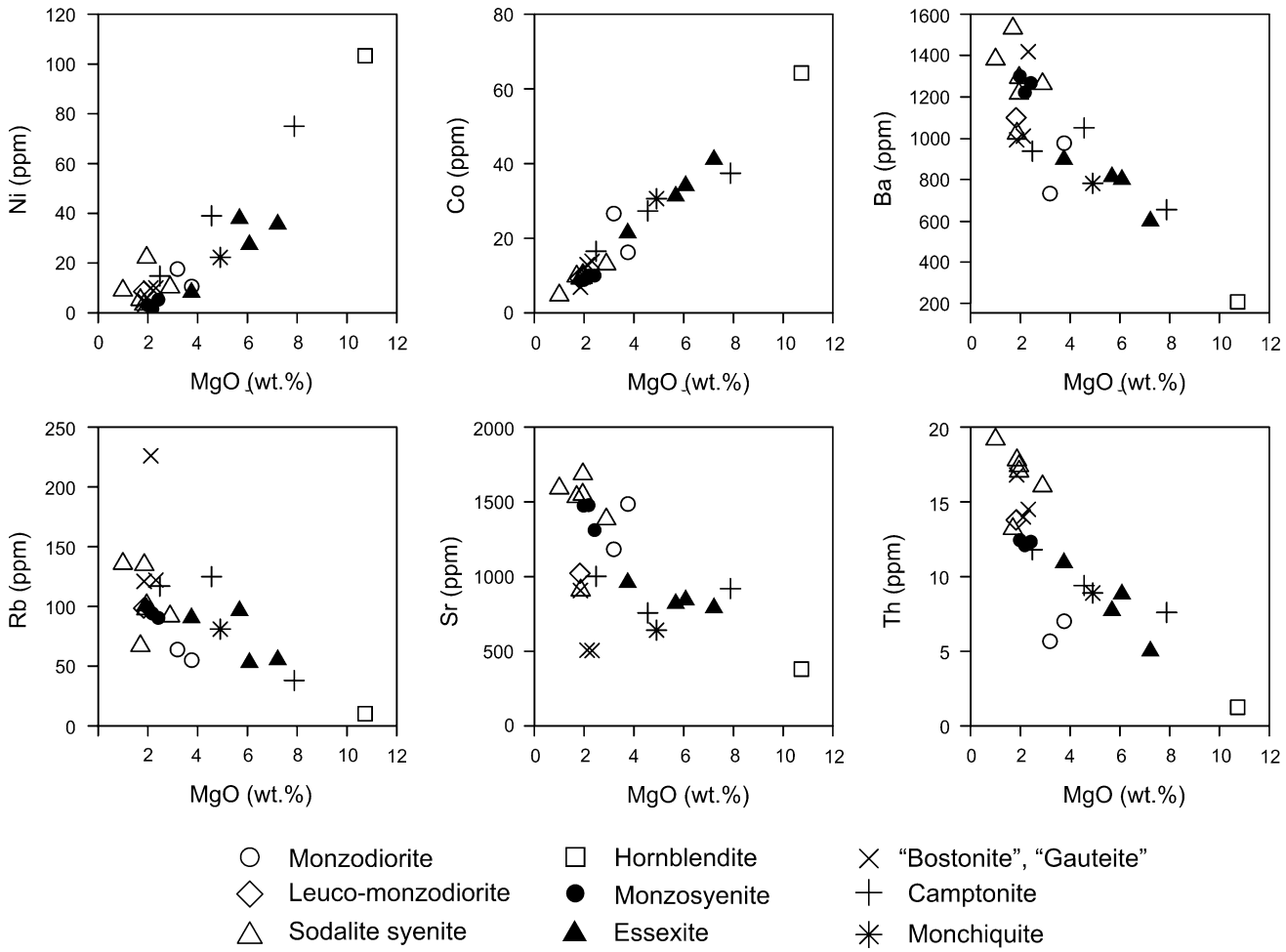

Fig. 14 MgO (wt%) versus selected trace element (ppm) variation diagrams for hypabyssal and dike rocks of the Roztoky Intrusive Complex

with decreasing Mg content, which is not the case of RIC suite (Fig. 14).

However, fractional crystallization processes alone cannot explain all compositional variations within the RIC suite, particularly the variations in trace elements and Sr–Nd isotopes. For example, the high contents of several incompatible trace elements (e.g., LREE, Th, Ba) in the sodalite syenites suggest that it is unlikely these rocks are simply products of continuous fractional crystallization of alkaline basaltic magma and may point to assimilation of crustal material. To provide more constraints on the role of crustal contamination, the importance of fractional crystallization (FC), assimilation–fractional crystallization (AFC) and mixing processes was examined. For FC process, the Rayleigh fractionation model was used (Allègre et al. 1977), the AFC model was tested by a procedure from DePaolo (1981), and for mixing of two components (parent magma and continental crust), a model of Powell (1984) was used. To test these models, elements with different degrees of compatibility during magma fractionation were selected. Cobalt is assumed as a typical compatible element (note its positive correlation with MgO; Fig. 14), and La is assumed as a typical incompatible element. The results were discussed in combination with Sr–Nd isotopic composition of the studied rocks. The essexite sample S-25 is assumed to be the composition closest to the expected parental magma on the basis of the highest temperature and pressure estimate, the highest MgO and the lowest SiO_2 contents. The composition of bulk continental crust (Rudnick and Gao 2003) was chosen as hypothetical assimilant. The mass ratio of assimilant/mass fractionated used in our AFC model is 0.7. The modeled FC, AFC and mixing paths constructed using FC–AFC–FCA Mixing modeler (Ersoy and Helvaci 2010) are shown in Fig. 15. Most of the hypabyssal rocks and lamprophyres dikes of the RIC suite plot along FC and AFC calculated curves (Fig. 15), and it is clear that the Co–La variation in RIC suite cannot be explained by simple mixing of two different components (e.g., S-25 and bulk continental crust). The essexite, monzodiorite and most of the lamprophyre dikes (except

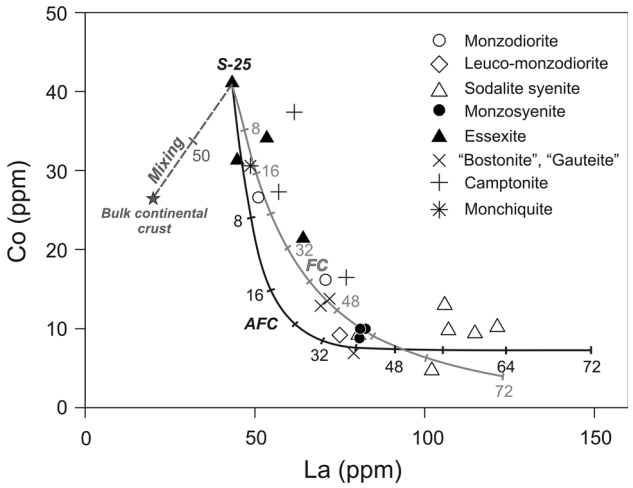

Fig. 15 Cobalt versus lanthanum diagram for samples of the Roztoky Intrusive Complex. Shown are calculated data trends for fractional crystallization (FC; *solid gray line*), assimilation–fractional crystallization (AFC; *solid black line*), and mixing of parental melt with assimilant (*dashed line*). As a parental magma composition, essexite sample S-25 (Mg#56) was chosen. Bulk continental crust (Rudnick and Gao 2003) represents an assimilant (indicated as *asterisk*). For details see the text

"bostonite" S-32 and camptonite S-43) can be accounted for by ~8–45 % of suggested parent magma crystallization without any contribution of crustal material. In contrast, monzosyenite and leuco-monzodiorite composition with variable Sr isotopic composition can be explained either by FC process with ~50 % of parental magma crystallization or by AFC process with lower ~35–40 % crystallization of parental magma. However, the latter is not supported with Nd isotopic data of these rocks overlapping with essexite and most of the lamprophyre dikes. The Co–La variation in sodalite syenites may suggests significant contribution of crustal material to their magmas, but this is not consistent with highly variable Sr–Nd isotopic composition with much of the sodalite syenite characterized by the highest ε_{Nd} among all studied rocks (Table 7; Fig. 13). Therefore, the fractional crystallization and/or assimilation–fractional crystallization was likely accompanied by other processes such as the late-magmatic transfer of volatile fluids containing Zr, U, Th and REE as implied by the occurrence of rare minerals, which concentrate these elements (Zr minerals) in the RIC concentrated in evolved differentiates as sodalite syenite and tinguaites (Ulrych et al. 1992).

The Sr–Nd isotopic compositions (Fig. 13) provide further constraints on the evolution of the RIC suite. Except monzosyenites with highly radiogenic $^{87}Sr/^{86}Sr$, all rocks fall in the depleted mantle field, and most of them plot in the least depleted portion of a data field for syn-rift Cenozoic volcanic rocks of the Bohemian Massif (Ulrych et al. 2011). However, large variations in the Sr–Nd isotopic compositions of individual rock types in spite of their similar petrography and whole-rock chemistry suggest variable crustal contributions and/or a heterogeneous mantle source. However, the former is not consistent with trace element AFC model employed above, in spite of the presence of crustal xenoliths (carboniferous and upper cretaceous sediments, Saxothuringian gneisses and altered granites, Ulrych et al. 2000) in the RIC hypabyssal rocks and dikes. In contrast, the latter is likely as $^{87}Sr/^{86}Sr$ ratios of 0.70314–0.70399 in mantle xenoliths from Cenozoic volcanic rocks (Blusztajn and Shimizu 1994; Ackerman et al. 2007; Ackerman, unpubl. data), and the presence of metasomatized mantle xenoliths in the volcanic rocks of the České středohoří Mts. Complex (Ackerman et al. 2013) may indicate heterogeneities in the subcontinental mantle. However, the RIC rocks with high $^{87}Sr/^{86}Sr$ (e.g., monzosyenite) may also have been modified by the late-stage magmatic fluids associated with evolution of the RIC.

Conclusions

Petrographic characteristics, major and trace element composition, as well as Sr–Nd isotopic data on monzodiorite–essexite–sodalite syenite suites and the associated dike swarms of the RIC suggest that they are genetically linked. The magmatic rhythmic layering of the RIC intrusions defined by the alternation in bands with different textures, different proportions of felsic to mafic minerals and different clinopyroxene/biotite ratios is probably due to flowage differentiation of the magma at deeper crustal levels. Trace element modeling shows that fractional crystallization (FC) and assimilation–fractional crystallization (AFC) processes could have played an important role in the evolution of the RIC rocks. The essexite, monzodiorite, monzosyenite, leuco-monzodiorite and most of the lamprophyre camptonite, monchiquite and maenite dikes can be best explained by ~8–50 % crystallization of essexite parent magma (the most depleted sample of essexite in terms of trace element composition) without no or limited contribution of crustal material. On the other hand, trace element composition of sodalite syenite is not consistent either with FC or AFC models, suggesting that their composition was most likely affected by the late-magmatic fluids. Large variations in the Sr–Nd isotopic compositions of the individual RIC rock cannot be explained by variable crustal contributions to the RIC parental melts, but rather reflect heterogeneous mantle source.

Acknowledgments This research was supported by the Grant Agency of the Academy of Sciences of the Czech Republic project

IAA300130902 and falls within the Research Programme of the Institute of Geology, v. v. i., RVO67985831. Financial support of Ministry of Education (project MSM 0021620855 of the Charles University) is greatly acknowledged. We are indebted to P. Špaček, Institute of Geophysics AS CR, v. v. i. for many useful discussion of the deep structure of the Bohemian Massif, L. Strnad (Faculty of Science, Charles University in Prague) and V. Böhmová Institute of Geology AS CR, v. v. i., Prague) who carried out chemical analyses, and J. Pavková and J. Rajlichová (Institute of Geology AS CR, v. v. i., Prague) for technical assistance. The paper benefited from detailed reviews by Michele Lustrino and John Greenough.

Appendix 1

See Table 8.

Table 8 Sample localities, geological and petrographic characteristics of the hypabyssal and dike rocks of the Roztoky Intrusive Complex

Sample	Location	N	E	Geological position	Lithology	Petrographic characteristics
S-1	"Köhlergrund" Valley in Roztoky, boulders at mouth of the gallery Anna	50°41′27″	14°11′11″	Marginal part of the Roztoky stock	Biotite-clinopyroxene leuco-monzodiorite, fine-grained	Heterogeneous, equigranular, rarely porphyritic, partly with vertical rhythmic layering, fine-grained, hypidiomorphic granitic to prismatic texture/*Plg* + *K-fsp* + *bi/cpx (phenocrysts)* ± *amph*, *mag*, *ilm*, *tit*, *ap*, *ep*
S-2	"Köhlergrund" Valley in Roztoky, boulders below the gallery Anna	50°41′25″	14°11′11″	Marginal part of the Roztoky stock	Clinopyroxene-biotite monzodiorite, fine- to medium-grained	
S-3	Vysoký kopec Hill, the railroad-cutting at the Povrly-Roztoky station	50°41′15″	14°11′12″	Central part of the Roztoky stock	Biotite monzodiorite, medium-grained	
S-10	Lícha Hill at Malé Březno, outcrops and boulders at the hill top	50°40′39″	14°11′24″	Boulders, apical part of the main outcrop of the Lícha stock?	Hornblende-biotite(bi?)-clinopyroxene essexite, medium-grained	Heterogeneous, dark types are fine-grained equigranular with hypidiomorphic texture, light types are prevalently of prismatic texture transiting to porphyritic to coarse-grained pegmatoidal (cpx) types/ *Plg* + *K-fsp* + *bi/cpx* (*phenocrysts*) ± *amph*, *mag*, *ilm*, *tit*, *ap*, *ep*
S-22	Lícha Hill at Malé Březno, outcrops and boulders at the hill slope	50°40′31″	14°11′07″	Boulders, lower, SW part of the circular outcrop Lícha stock	Biotite-clinopyroxene essexite, medium-grained	
S-23	Lícha Hill at Malé Březno, outcrops and boulders at the hill slope	50°40′35″	14°11′06″	Boulders, higher, SW part of the circular outcrop of the Lícha stock	Biotite-clinopyroxene essexite, medium-grained	
S-24	Lícha Hill at Malé Březno, outcrops and boulders at the hill slope	50°40′38″	14°11′21″	Boulders, apical part of the main outcrop of the Lícha stock	Clinopyroxene essexite, porphyritic	
S-25	Lícha Hill at Malé Březno, outcrops and boulders at the hill slope	50°40′27″	14°10′46″	Boulders, foot of the SW part of the circular outcrop of the Lícha stock	Clinopyroxene essexite, medium-grained	
S-4	Hradiště Hill at Svádov, abandoned medium quarry II	50°39′59″	14°16′58″	Central part of the Hradiště stock	Analcime/sodalite syenite, fine-grained with clinopyroxene phenocrysts	Overall homogeneous, equigranular, rarely porphyritic, fine-grained partly coarse-grained hypidiomorphic granitic to prismatic texture, sodalite replaced by analcime/*K-fsp* + *sod/analc* + *cpx* + *hbl* (xenocrysts?) ± *plg*, *tit*, *mag*, *ap*
S-18	Hradiště Hill at Svádov, abandoned upper quarry III	50°39′55″	14°06′51″	Central part of the Hradiště stock	Anacime/sodalite syenite, medium-grained, spotted	
S-9	Olešnice brook valley at Svadov-Olešnice, abandoned quarry	50°39′55″	14°07′32″	Marginal "Olešnice part" of the Hradiště stock	Analcime/sodalite syenite, fine-grained	
S-8	Stříbrníky in Ústí n.L., boulders near the garden colony	50°40′19″	14°02′51″	Stříbrníky stock (?)	Analcime/sodalite syenite, fine-grained	
S-5	"Giegelberg" Hill at Zubrnice, abandoned quarry	50°38′54″	14°12′42″	Central part of the "Giegelberg" stock	Analcime/sodalite syenite, fine-grained with hbl cumulate/ xenocrysts (?)	
S-6	"Giegelberg" Hill at Zubrnice, abandoned quarry	50°38′54″	14°12′42″	Central part of the "Giegelberg" stock	(Clinopyroxene)-hornblendite cumulate/xenolith (hbl ≫ cpx)	Mostly medium to coarse-grained confining structure, rarely pencil structure of subparallel coarse-grained blades of hbl/*Hbl* + *cpx* ± *plg*, *ol*, *mag*, *tit*, *ap*

Table 8 continued

Sample	Location	N	E	Geological position	Lithology	Petrographic characteristics
S-7	Vinice Hill (also Křížový vrch Hill) at Býčkovice, abandoned small quarry	50°33′43″	14°13′07″	Marginal part of the main outcrop of the Býčkovice stock	Sodalite-bearing monzosyenite	Partly inhomogeneous with irregular banding, mostly equigranular, fine-grained, rarely porphyritic hypidiomorphic granitic to prismatic texture, sodalite partly replaced by analcime/*K-fsp* + *sod*/*analc* + *cpx* ± *plg*, *tit*, *mag*, *ap*
S-16	Vinice Hill at Býčkovice, small outcrop at the NE edge of the top	50°33′41″	14°13′16″	Central part of the main outcrop of the Býčkovice stock	Sodalite-bearing monzosyenite	
S-17	Vinice Hill at Býčkovice, boulders and outcrops at the top of the hill	50°33′41″	14°13′12″	Central part of the main outcrop of the Býčkovice stock	Sodalite-bearing monzosyenite	
S-30	Dobkovice, abandoned "Zajíček" quarry, right wall	50°42′38″	14°11′34″	Subvertical dike 0.5 to 1 m thick in basanite	Monchiquite (lamprophyre)	Porphyritic, *cpx*, (*hbl*) phenocrysts in fine-grained matrix (*cpx*, *hbl*?, *phl*?, *sod*/*analc*, *glass*, *mag*, *ap*), cavities with *zeol*, *carb*
S-31	Dobkovice, abandoned "Zajíček" quarry, right wall	50°42′38″	14°11′34″	Subvertical dike 1 m thick in basanite	Camptonite (lamprophyre)	Porphyritic, *hbl*, *phl* ± *cpx*, *leuc*, *plg* phenocrysts in fine-grained matrix (*hbl*, *cpx*, *phl*, *plg*, *sod*/*analc*, *mag*, *ap*), cavities with *zeol*, *carb*
S-43	SE end of the village Leština, abandoned small quarry	50°39′22″	14°12′18″	Subvertical dike 3 to 5 m thick in Cretaceous sandstones	Camptonite (lamprophyre)	
S-34	Těchlovice, active quarry of Tarmac Group, first etage, left	50°42′26″	14°12′04″	Subvertical dike 1 m thick in basanite	Camptonite to "gauteite"	Porphyritic, *hbl*, *cpx*, *phl*, *plg* ± *sod* phenocrysts in fine-grained matrix (*plg*, *k-fsp*, *hbl*, *cpx* ± *glass*, *mag*, *ap*) Abundant cavities with *zeol*, *carb*
S-33	Těchlovice, active quarry of Tarmac Group, first etage, left	50°42′26″	14°12′04″	Subvertical dike 1 m thick in basanite	"Gauiteite"	
S-35	Těchlovice, active quarry of Tarmac Group, first etage, left	50°42′26″	14°12′04″	Subvertical dike 1 m thick in basanite	"Gauteite"	
S-32	Těchlovice, active quarry of Tarmac Group, first etage, left	50°42′26″	14°12′04″	Subvertical dike 0.5 m thick in basanite	"Bostonite"	Porphyritic, *plg* ± *cpx*, *hbl*, *bi*, *sod* phenocrysts in fine-grained matrix (*K-fsp*, *plg* ± *bi*, *hbl*, *sod*, *mag*, *tit*, *ap*)

Appendix 2

See Fig. 16.

Fig. 16 Photomicrographs of representative hypabyssal rocks of the Roztoky Intrusive Complex. All images taken in cross-polarized light except where indicated otherwise. The field of view corresponds to 8.83 × 6.65 mm in all photographs. **a** Clinopyroxene essexite, dark medium-grained, Lícha Hill (boulders) at Malé Březno (sample S-25); **b** clinopyroxene essexite, porphyritic, Lícha Hill (boulders) at Malé Březno (sample S-24); **c** clinopyroxene–biotite monzodiorite, fine- to medium-grained, "Köhlergrund" Valley in Povrly-Roztoky (sample S-2); **d** biotite monzodiorite, medium-grained, Vysoký kopec Hill, the railroad-cutting at the Povrly-Roztoky station (sample S-3); **e** analcime/sodalite syenite, fine-grained with clinopyroxene phenocrysts, Hradiště Hill at Svádov (sample S-4); **f** analcime/sodalite syenite, fine-grained with hornblende disaggregated cumulate (?), "Giegelberg" Hill abandoned quarry at Zubrnice (sample S-5); **g** clinopyroxene–hornblendite cumulate/xenolith (hornblende ≫ clinopyroxene), "Giegelberg" Hill, abandoned quarry at Zubrnice (plane-polarized light; sample S-6); **h** sodalite-bearing monzosyenite, Vinice Hill (*top*) at Býčkovice (sample S-16)

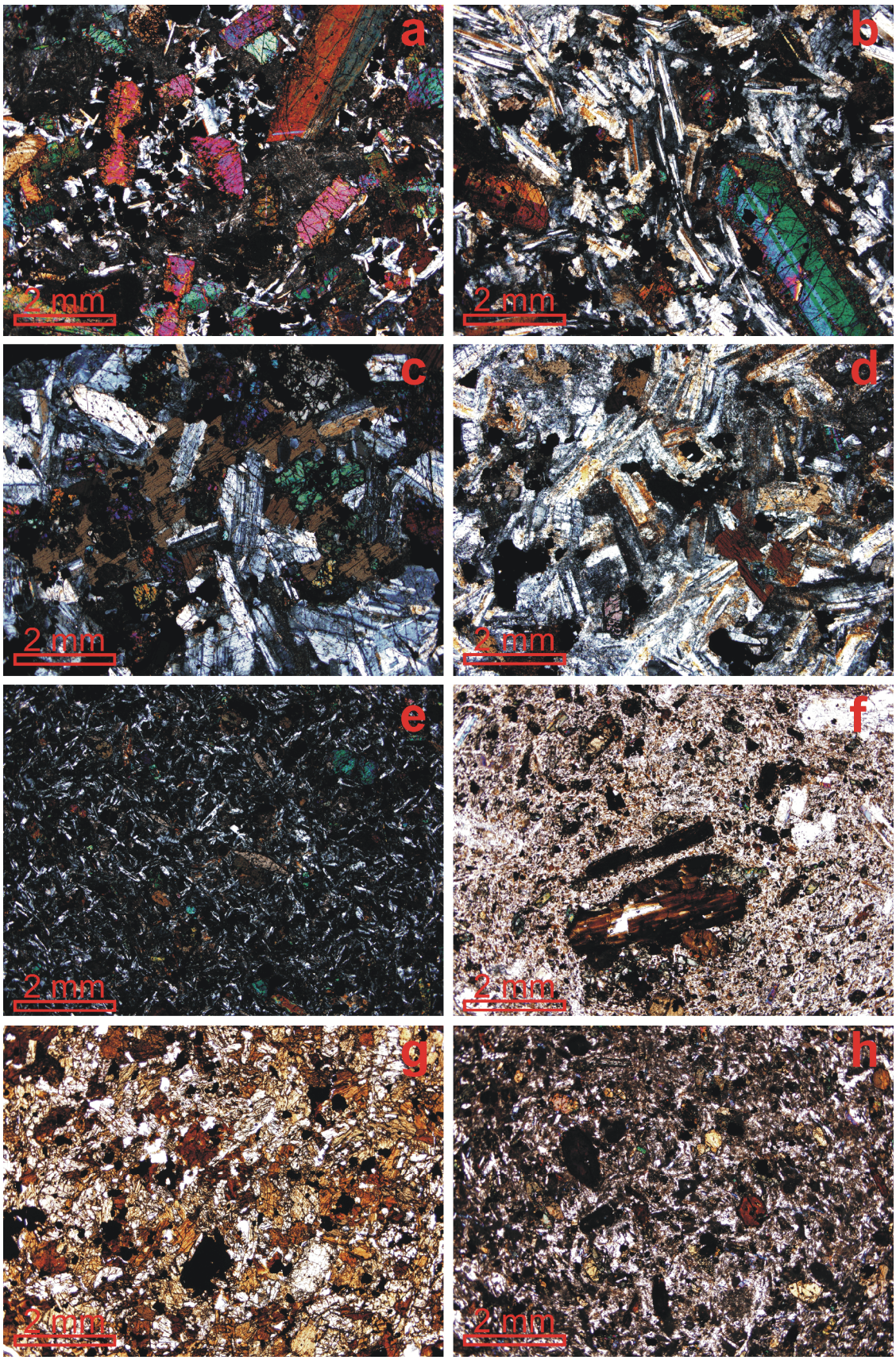
a
2 mm
b
2 mm
c
2 mm
d
2 mm
e
2 mm
f
2 mm
g
2 mm
h
2 mm

References

Ackerman L, Mahlen N, Jelinek E, Medaris LG, Ulrych J, Strnad L, Mihaljevic M (2007) Geochemistry and evolution of subcontinental lithospheric mantle in Central Europe: evidence from peridotite xenoliths of the Kozakov volcano, Czech Republic. J Petrol 48:2235–2260

Ackerman L, Špaček P, Ulrych J (2013) Petrology and geochemistry of mantle xenoliths from České Středohoří Mts. and Lusatia, Bohemian Massif. In: Büchner J, Rapprich V, Tietz O (eds) Basalt 2013 Abstracts and Excursion Guides, pp 39–40

Allègre CJ, Treuil M, Minster JF, Minster JB, Albarede F (1977) Systematic use of trace element in igneous process. Part I: fractional crystallization processes in volcanic suites. Contrib Mineral Petrol 60:57–75

Alibert C, Leterrier J, Panasiuk M, Zimmermann JL (1987) Trace and isotope geochemistry of the alkaline Tertiary volcanism in southwestern Poland. Lithos 20(4):311–321

Babuška V, Plomerová J (1992) The lithosphere in central Europe—seismological and petrological aspects. Tectonophysics 207:141–163

Babuška V, Plomerová J (2001) Subcrustal lithosphere around the Saxothuringian–Moldanubian Suture Zone—a model derived from anisotropy of seismic wave velocities. Tectonophysics 332:185–199

Babuška V, Plomerová J (2010) Mantle lithosphere control of crustal tectonics and magmatism of the western Ohře (Eger) Rift. J Geosci 55:171–186

Babuška V, Plomerová J, Fischer T (2007) Intraplate seismicity in the western Bohemian Massif (central Europe): a possible correlation with a paleoplate junction. J Geodyn 44:149–159

Bellon H, Bůžek Č, Gaudant J, Kvaček Z, Walther H (1998) The České středohoří magmatic complex in Northern Bohemia ^{40}K–^{40}Ar ages for volcanism and biostratigraphy of the Cenozoic freshwater formations. Newsl Stratigr 36:77–103

Bhattacharji S (1966) Flowage differentiation in Mount Johnson stock, Monteregian Hills, Canada. Am Geophys Union 47:196

Bhattacharji S, Nehru CE (1972) Igneous differentiation model for origin of Mount Johnson, a zoned Monteregian intrusion, Quebec, Canada. Int Geol Congr XXIV Sess 15:3–17

Blusztain J, Hart SR (1989) Sr, Nd and Pb isotopic character of Tertiary basalts from southwest Poland. Geochim Cosmochim Acta 53:2689–2696

Blusztajn J, Shimizu N (1994) The trace-element variations in clinopyroxenes from spinel peridotite xenoliths from southwest Poland. Chem Geol 111:227–243

Bräuer K, Kämpf H, Niedermann S, Strauch G (2005) Evidence for ascending upper mantle-derived melt beneath the Cheb basin, central Europe. Geophys Res Lett 32:L08303. doi:10.1029/2004GL022205

Buddington AF, Lindsley DH (1964) Iron-titanium oxide minerals and synthetic equivalents. J Petrol 5:310–357

Cajz V, Vokurka K, Balogh K, Lang M, Ulrych J (1999) The České středohoří Mts. – volcanostratigraphy and geochemistry. Geolines 9:21–28

Cox KG, Bell JD, Pankhurst RJ (1979) The interpretation of igneous rocks. Allen and Unwin, London

DePaolo DJ (1981) Trace element and isotopic effects of combined wall-rock assimilation and fractional crystallization. Earth Planet Sci Lett 53:189–202

Dèzes P, Schmid SM, Ziegler PA (2004) Evolution of the European Cenozoic rift system: interaction of the Alpine and Pyrenean orogens with their foreland lithosphere. Tectonophysics 389:1–22

Dons JA, Larsen BT (1978) The Oslo paleorift. A review and guide to excursions. Universitetsforlaget, Trondheim

Eby GN (1984) Monteregian Hills I. Petrography, major and trace element geochemistry, strontium isotopic chemistry of The Western Instrusions: Mounts Royal, St. Bruno, and Johnson. J Petrol 25:421–452

Eby GN (1985a) Monteregian Hills II. Petrography, major and trace element geochemistry, strontium isotopic chemistry of The Eastern Intrusions: Mounts Shefford, Brome, and Megantic. J Petrol 26:418–448

Eby GN (1985b) Age relations, chemistry, and petrogenesis of mafic alkaline dikes from the Monteregian Hills and younger White Mountain Igneous provinces. Can J Earth Sci 22:1103–1111

Eby GN (1987) The Monteregian Hills and White Mountain alkaline igneous provinces, eastern North America. In: Fitton JG, Upton BGJ (eds) Alkaline igneous rocks. Geol Soc Spec Publ 30. Blackwell Sci. Publ., Oxford, pp 433–447

Ersoy Y, Helvaci C (2010) FC–AFC–FCA and mixing modeler: a Microsoft Excel & spreadsheet program for modeling geochemical differentiation of magma by crystal fractionation, crustal assimilation and mixing. Comput Geosci 36:383–390

Foulger GR, Meyer R (2007) The European Cenozoic volcanic province; the type example of an implausible plume (IMP)? EOS Trans Am Geophys Union 88:52

Franke W (1989) Variscan plate tectonics in Central Europe—current ideas and open questions. Tectonophysics 169:221–228

Geissler WH, Kind R, Yuan X (2008) Upper mantle and lithospheric heterogeneities in central and eastern Europe as observed by teleseismic receiver functions. Geophys J Int 181(2):604–634

Geissler WH, Kämpf H, Skácelová Z, Plomerová J, Babuška V, Kind R (2012) Lithosphere structure of the NE Bohemian Massif (Sudetes)—a teleseismic receiver function study. Tectonophysics 564–565:12–37

Goes S, Spakman W, Bijwaard H (1999) A lower mantle source for central European volcanism. Science 286:1928–1931

Granet M, Wilson M, Achauer U (1995) Imaging mantle plumes beneath the French Massif Central. Earth Planet Sci Lett 136:199–203

Guo F, Fan W, Wang Y, Zhang M (2004) Origin of early Cretaceous calc-alkaline lamprophyres from the Sulu orogen in eastern China: implications for enrichment processes beneath continental collisional belt. Lithos 78:291–305

Hegner E, Walter HJ, Satir M (1995) Pb–Sr–Nd isotopic composition and trace element geochemistry of megacrysts and melilitites from the Tertiary Urach volcanic field: source composition of small volume melts under SW Germany. Contrib Mineral Petrol 122:322–335

Henry DJ, Guidotti CV, Thomson JA (2005) The Ti-saturation surface for low-to-medium pressure metapelitic biotite: implications for geothermometry and Ti-substitution mechanisms. Am Mineral 90:316–328

Heuer B, Kämpf H, Kind R, Geissler WH (2007) Seismic evidence for whole lithosphere separation between Saxothuringian and Moldanubian tectonic units in central Europe. Geophys Res Lett 34:L09304. doi:10.1029/2006GL029188

Hibsch JE (1926) Erläuterungen zur geologischen Übersichtskarte des böhmischen Mittelgebirges un der unmittelbar angrenzenden Gebiete zugleich in allgemein verständlicher geologischer Führer. Freier Lehrerverein, Tetschen a.d. Elbe.

Holub FV, Rapprich V, Erban V, Pecskay Z, Mlčoch B, Miková J (2010) Petrology and geochemistry of the Tertiary alkaline intrusive rocks at Doupov, Doupovské hory Volcanic Complex (NW Bohemian Massif). J Geosci 55:251–278

Hrubcová P, Środa P, CELEBRATION 2000 Working Group (2008) Crustal structure at the easternmost termination of the Variscan belt based on CELEBRATION 2000 and ALP 2002 data. Tectonophysics 460:55–75

Hoernle K, Zhang Y-S, Graham D (1995) Seismic and geochemical evidence for large-scale mantle upwelling beneath the eastern Atlantic and western and central Europe. Nature 374:34–39

Jacobsen SB, Wasserburg GJ (1980) Sm–Nd isotopic evolution of chondrites. Earth Planet Sci Lett 50:139–155

Jelínek E, Souček J, Tvrdý J, Ulrych J (1989) Geochemistry and petrology of alkaline dyke rocks of the Roztoky volcanic centre, České středohoří Mts., ČSSR. Chem Erde 49:201–217

Johnson WM, Maxwell JA (1981) Rock and mineral analysis. Wiley, New York

Keller J (1981) Carbonatitic volcanism in the Kaiserstuhl alkaline complex: evidence for highly fluid carbonatitic melts at the Earth's surface. J Volcanol Geoth Res 9:423–431

Kopecký L (1978) Neoidic taphrogenic evolution and young magmatism of the Bohemian Massif. Sbor Geol Věd Ř G 31:91–107

Kopecký L (1987a) The Roztoky pseudotachylite caldera in the České středohoří Mts., Czechoslovakia. In: Kopecký L (ed) Proceedings of first seminar on carbonatites and alkaline rocks Bohemian Massif and ambient region. Geological Survey, Prague, pp 119–156

Kopecký L (1987b) Isotopic composition and origin of carbonatites in alkaline-metasomatic and cognate rocks of the Bohemian Massif, Czechoslovakia. In: Kopecký L (ed) Proceedings of first seminar on carbonatites and alkaline rocks Bohemian Massif and ambient region. Geological Survey, Prague, pp 177–196

Leake BE, Woolley AR, Arps CES, Birch WD, Gilbert MC, Grice JD, Hawthorne FC, Kato A, Kisch HJ, Krivovichev VG, Linthout K, Laird J, Mandarino JA, Maresch WV, Nickel EH, Rock NMS, Schumacher JC, Smith DC, Stephenson NCN, Ungaretti L, Whittaker EJW, Youzhi G (1997) Nomenclature of amphiboles: report of the Subcommittee on amphiboles of the International Mineralogical Association, Commission on New Minerals and Mineral Names. Can Mineral 35:219–246

Le Bas MJ (1977) Carbonatite–nephelinite volcanism. An African case history. Wiley, London

Le Bas MJ (1987) Ultra-alkaline magmatism without rifting. Tectonophysics 143:75–84

Le Maitre RW (2002) Igneous rocks. A classification and glossary of terms: recommendations of the International Union of Geological Sciences Subcommission on the Systematics of Igneous Rocks, 2nd edn. Cambridge University Press, Cambridge

Lustrino M, Carminati E (2007) Phantom plumes in Europe and the circum-Mediterranean region. In: Foulger GR, Jurdy DM (eds) The origins of melting anomalies: plumes plates and planetary processes. Geol Soc Am Spec Pap 430:723–745

Lustrino M, Wilson M (2007) The circum-Mediterranean anorogenic Cenozoic igneous province. Earth-Sci Rev 81:1–65

McDonough WF, Sun S (1995) The composition of the Earth. Chem Geol 120:223–253

Michon L, Merle O (2001) The evolution of the Massif central rift. Spatio-temporal distribution of the volcanism. B Soc Geol Fr 172(2):201–211

Morimoto N, Fabries J, Ferguson AK, Ginzburg IV, Ross M, Seifert FA, Zussman L, Aoki K, Gottardi G (1988) Nomenclature of pyroxenes. Mineral Petrol 39:55–76

Mrlina J, Cajz V (2006) Subsurface structure of the volcanic centre of the České středohoří Mountains, North Bohemia, determined by geophysical survey. Stud Geophys Geod 50:75–88

Otten MT (1984) The origin of brown hornblende in the Artfjallet gabbro and dolerites. Contrib Mineral Petrol 86:189–199

Oyarzun R, Doblas M, López-Ruiz J, Cebrá J (1997) Opening of the central Atlantic and asymmetric mantle upwelling phenomena: implications for long-lived magmatism in western North Africa and Europe. Geology 25:727–730

Philpotts AR (1974) The Monteregian Province. In: Sörensen H (ed) The alkaline rocks. Wiley, London, pp 293–310

Pivec E, Ulrych J, Šrein V, Bendl J, Dobeš P, Žák K (1998) Epithermal Tertiary Pb–Zn–Cu (Ag, Te) mineralization in the Roztoky volcanic centre, České středohoří Mts., Czech Republic. Geol Carpath 49:139–146

Potts PJ (1995) A handbook of silicate rock analysis. Blackie Academic and Professional, London

Powell R (1984) Inversion of the assimilation and fractional crystallization (AFC) equations; characterization of contaminants from isotope and trace element relationships in volcanic suites. J Geol Soc London 141:447–452

Prodehl C, Müller S, Haak V (1995) The European Cenozoic rift system. In: Olsen KH (ed) Continental rifts: evolution, structure, tectonics. Elsevier, Amsterdam, pp 133–212

Putirka KD (2008) Thermometers and barometers for volcanic systems. In: Putirka KD, Tepley F (eds) Minerals, inclusions, and volcanic processes. Rev Mineral Geochem 61–120

Rieder M, Cavazzini G, D'yakonov YS, Frank-Kamenetskii VA, Gottardi G, Guggenheim S, Koval' PV, Müller G, Neiva AMR, Radoslovich EW, Robert JL, Sassi FP, Takeda H, Weiss Z, Wones DR (1998) Nomenclature of the micas. Can Mineral 36:905–912

Rock NMS (1978) Petrology and petrogenesis of the Monchique complex, southern Portugal. J Petrol 19:171–214

Rock NMS (1991) Lamprophyres. Blackie, Glasgow

Rudnick RL, Gao S (2003) Composition of continental crust. In: Rudnick RL (ed) Treatise on geochemistry, the crust. Elsevier, Oxford, pp 1–64

Schmidt MW (1992) Amphibole composition in tonalite as a function of pressure: an experimental calibration of the Al-in-hornblende barometer. Contrib Mineral Petrol 110:304–310

Shrbený O (1969) Tertiary magmatic differentiation in the central part of the České středohoří Mountains. Čas Mineral Geol 14:285–298

Shrbený O (1995) Chemical composition of young volcanites of the Czech Republic. Czech Geol Surv Papers 4. Czech Geological Survey, Prague, pp 1–53

Sommerauer J, Katz-Lehnert K (1985) A new partial substitution mechanism of CO_3^{2-}/CO_3OH^{3-} and SiO_4^{4-} for the PO_4^{4-} group in hydroxyapatite from Kaiserstuhl alkaline complex (SW-Germany). Contrib Mineral Petrol 91:360–368

Strnad L, Mihaljevič M, Šebek O (2005) Laser ablation and solution ICP-MS determination of rare earth elements in USGS BIR-1G, BHVO-2G and BCR-2G glass reference material. Geostand Geoanal Res 29:303–314

Taylor HP, Frechen J, Degens ET (1967) Oxygen and carbon isotope studies of carbonatites from the Laacher See District, West Germany and Alnö District, Sweden. Geochim Cosmochim Acta 31:407–430

Tischendorf G, Rieder M, Förster HJ, Gottesmann B, Guidotti CV (2004) A new graphical presentation and subdivision of potassium micas. Mineral Mag 68:649–667

Tischendorf G, Förster HJ, Gottesmann B, Rieder M (2007) True and brittle micas: composition and solid-solution series. Mineral Mag 71:285–320

Tröger WE (1935) Spezielle Petrographie der Eruptivgesteine. Ein Nomenklatur–Kompendium. Schweizerbartsche Verlagsbuchhandlung, Stutgart

Ulianov A, Müntener O, Ulmer P, Pettke T (2007) Entrained macrocryst minerals as a key to the source region of olivine nephelinites: Humberg, Kaiserstuhl, Germany. J Petrol 48(6):1079–1118

Ulrych J (1983) Chemical composition of sector-zoned clinopyroxene from monchiquite and rongstockite, České středohoří Mts. Acta Univ Carolinae Geol Rost Vol:117–131

Ulrych J (1998) Geochemistry of subvolcanic alkaline rocks series of the Roztoky Intrusive Centre, České středohoří Mts., Bohemia. Erlangen Beitr Petrogr Mineral 8:1–42

Ulrych J, Balogh K (2000) Roztoky Intrusive Centre in the České středohoří Mts.: differentiation, emplacement, distribution, orientation and age of dyke series. Geol Carpath 51:383–397

Ulrych J, Novák P (1989) Geochemistry of the Býčkovice monzosyenitic body, České středohoří Mts., Czechoslovakia. Acta Univ Carolinae Geol Fediuk Vol:139–163

Ulrych J, Pivec E (1997) Age related contrasting alkaline volcanic series in North Bohemia. Chem Erde 57:300–323

Ulrych J, Dostal J, Adamovič J, Jelínek E, Špaček P, Hegner E, Balogh K (2011) Recurrent Cenozoic volcanic activity in the Bohemian Massif (Czech Republic). Lithos 123:133–144

Ulrych J, Jelínek E, Řanda Z, Lloyd FE, Balogh K, Hegner E, Novák JK (2010) Geochemical characteristics of the high- and low-Ti basaltic rocks from the uplifted shoulder of the Ohře (Eger) Rift, Western Bohemia. Chem Erde–Geochem 70(4):319–333

Ulrych J, Novák JK, Lang M, Balogh K, Hegner E, Řanda Z (2006) Petrology and geochemistry and K–Ar ages for Cenozoic tinguaites from the Ohře/Eger Rift (NW Bohemia). Neues Jb Miner Abh 183:41–61

Ulrych J, Novák JK, Lang M, Balogh K, Kropáček V (1999) Cenozoic intraplate volcanic rock series of the Bohemian Massif: a review. Geolines 9:123–129

Ulrych J, Pivec E, Fiala J, Lang M (1983) Petrology of the alkaline subvolcanic rocks from the Roztoky area (České středohoří Mts.). Rozpr České Akad Věd, Řada Matematicko- přírodních věd, Academia, Prague, pp 1–84

Ulrych J, Pivec E, Höhndorf A, Balogh K, Bendl J, Rutšek J (2000) Rhyolites from the Roztoky Intrusive Centre, České středohoří Mts.: xenoliths or dyke rocks? Chem Erde 60:327–352

Ulrych J, Pivec E, Povondra P, Bendl J (1997) Geochemical and isotope characteristics of representative carbonates in young alkaline volcanites from northern Bohemia. J Czech Geol Soc 2:26–32

Ulrych J, Pivec E, Rychlý R, Rutšek J (1992) Zirconium mineralization of young alkaline volcanic rocks from northern Bohemia. Geol Carpath 43:91–95

Ulrych J, Svobodová J, Balogh K (2002) The source of Cenozoic volcanism in the České středohoří Mts., Bohemian Massif. Neues Jb Mineralogie Abh 177:133–162

Wedepohl KH (1985) Origin of the Tertiary basaltic volcanism in the northern Hessian depression. Contrib Mineral Petrol 89:122–143

Wilkinson JFG, Hensel J (1994) Nephelines and analcimes in some alkaline igneous rocks. Contrib Mineral Petrol 118:79–91

Wilson M, Downes H (1991) Tertiary–quaternary extension-related alkaline magmatism in western and central Europe. J Petrol 32:811–849

Wilson M, Patterson R (2001) Intraplate magmatism related to short-wavelength convective instabilities in the upper mantle: evidence from the Tertiary–Quaternary volcanic province of western and central Europe. In: Ernst RE, Buchan KL (eds) Mantle plumes: their identification through time. Geol Soc Am Spec Pap 352, Boulder, Colorado, pp 37–58

Wilson M, Downes H, Cebria J-H (1995) Contrasting fractionation trends in coexisting continental alkaline magma series, Cantal, Massif Central, France. J Petrol 32:811–849

Wilson M, Rosenbaum J, Ulrych J (1994) Cenozoic magmatism of the Ohře rift, Czech Republic: geochemical signatures and mantle dynamics. Int Volcanol Congress 1994, Abstracts, Ankara

Wimmenauer W (1974) The alkaline province of Central Europe and France. In: Sørensen H (ed) The alkaline rocks. Wiley, London, pp 286–291

Ziegler PA (1990) Geological atlas of Western and Central Europe, 2nd edn. Shell Internationale Petroleum Maatschappij B.V. and Geological Society London, The Hague

Ziegler PA (1994) Cenozoic rift system of Western and Central Europe: an overview. Geol Mijnbouw 73:99–127

Ziegler PA, Dézes P (2006) Crustal evolution of Western and Central Europe. In: Gee DG, Stephenson RA (eds) European lithosphere dynamics. Geol Soc Mem 32:43–56